

OFFICE OF CIVILIAN RADIOACTIVE WASTE MANAGEMENT
 ANALYSIS/MODEL COVER SHEET
Complete Only Applicable Items

1. QA: QA
 Page: 1 of 69

| | |
|---|--|
| 2. <input checked="" type="checkbox"/> Analysis <input type="checkbox"/> Engineering <input checked="" type="checkbox"/> Performance Assessment <input type="checkbox"/> Scientific | 3. <input type="checkbox"/> Model <input type="checkbox"/> Conceptual Model Documentation <input type="checkbox"/> Model Documentation <input type="checkbox"/> Model Validation Documentation |
|---|--|

4. Title: Initial Cladding Condition

5. Document Identifier (including Rev. No. and Change No., if applicable):
 ANL-EBS-MD-000048, Rev. 00A

| | |
|-------------------------|--|
| 6. Total Attachments: 3 | 7. Attachment Numbers - No. of Pages in Each: Attachments: I - 1 page, II - 4 pages, III - 18 pages |
|-------------------------|--|

| | Printed Name | Signature | Date |
|-------------------------|----------------|-----------|------|
| 8. Originator | E. R. Siegmann | | |
| 9. Checker | H. Anderson | | |
| 10. Lead/Supervisor | R. Rechar | | |
| 11. Responsible Manager | R. MacKinnon | | |

12. Remarks:
 This document is associated with AMR F0045.

OFFICE OF CIVILIAN RADIOACTIVE WASTE MANAGEMENT
ANALYSIS/MODEL COVER SHEET
Complete Only Applicable Items

1. QA: QA
Page: 1 of: 69

**OFFICE OF CIVILIAN RADIOACTIVE WASTE
MANAGEMENT
ANALYSIS/MODEL REVISION RECORD**
Complete Only Applicable Items

1. Page: 3 of: 69

2. Analysis or Model Title: Initial Cladding Condition

3. Document Identifier (including Rev. No. and Change No., if applicable): ANL-EBS-MD-000048 Rev. 00

4. Revision/Change No.

5. Description of Revision/Change

00A

Check Copy

CONTENTS

| | Page |
|---|------|
| 1. 1 | |
| 1. PURPOSE | 8 |
| 2. QUALITY ASSURANCE | 8 |
| 3. COMPUTER SOFTWARE AND MODEL USAGE | 8 |
| 4. INPUTS | 8 |
| 4.1/ DATA AND PARAMETERS | 8 |
| 4.2 CRITERIA | 10 |
| 4.3 CODES AND STANDARDS | 11 |
| 5. ASSUMPTIONS | 11 |
| 5.1 ASSUMPTIONS FOR CLADDING TYPES | 11 |
| 5.2 ASSUMPTIONS FOR ROD INTERNAL PRESSURE | 11 |
| 5.3 ASSUMPTIONS FOR SURFACE CORROSION | 12 |
| 5.4 ASSUMPTIONS FOR CRACK SIZE DISTRIBUTION | 13 |
| 5.5 ASSUMPTIONS FOR ROD FAILURE DURING REACTOR OPERATION | 13 |
| 5.6 ASSUMPTIONS FOR ROD FAILURE DURING DRY STORAGE | 14 |
| 5.7 ASSUMPTIONS FOR ROD FAILURE DURING FUEL SHIPMENT | 14 |
| 6. ANALYSIS/MODEL | 15 |
| 6.1 CLADDING TYPES | 15 |
| 6.2 BURNUP | 17 |
| 6.3 ROD INTERNAL PRESSURE | 18 |
| 6.3.1 Initial Fill Pressure | 18 |
| 6.3.2 Fission Gas Production | 19 |
| 6.3.3 Fission Gas Release Fraction | 19 |
| 6.3.4 Helium Production | 24 |
| 6.3.5 Free Gas Volume | 25 |
| 6.3.6 Plenum Pressure Distribution | 26 |
| 6.4 SURFACE CORROSION | 27 |
| 6.5 HYDRIDE FORMATION | 28 |
| 6.6 CRACK SIZE DISTRIBUTION | 29 |
| 6.7 CLADDING STRESS | 30 |
| 6.8 RODS FAILURES DURING REACTOR OPERATION | 32 |
| 6.8.1 BWR Rod Failure Distribution | 32 |
| 6.8.2 PWR Rod Failure Distribution | 33 |
| 6.8.3 Incipient Failures | 35 |
| 6.8.4 Combined CCDF | 36 |
| 6.8.5 Corroborating Data | 36 |
| 6.8.6 Future Fuels | 37 |

| | | |
|--------|---|----|
| 6.9 | ROD FAILURE DURING SPENT FUEL POOL STORAGE..... | 38 |
| 6.10 | ROD FAILURE DURING DRY STORAGE..... | 39 |
| 6.10.1 | Creep Failures in Dry Storage and Transportation..... | 40 |
| 6.10.2 | DHC Failures in Dry Storage..... | 42 |
| 6.11 | ROD FAILURE DURING FUEL SHIPMENT..... | 44 |
| 7. | CONCLUSIONS..... | 46 |
| 8. | REFERENCES..... | 48 |
| 9. | ATTACHMENTS..... | 69 |

FIGURES

| | Page |
|--|------|
| Figure 1. Equilibrium Cycle Discharge vs. Calendar Year (from DOE 1996) | 55 |
| Figure 2. Expected Burnup Distribution for PWR Assemblies | 55 |
| Figure 3. Distribution of Assembly Burnup | 56 |
| Figure 4. Fission Gas Release for U.S. PWR fuel Rods (from Garde 1986)..... | 56 |
| Figure 5. Fission Gas Release vs. Burnup (from Manzel and Coquerelle 1997) | 57 |
| Figure 6. Helium Pressure from Alpha Decay (From Manaktala 1993)..... | 57 |
| Figure 7. Fuel Rod Void Volume Change as a Function of Rod Average Burnup (from Smith et al. 1994) . | 58 |
| Figure 8. Rod Internal Pressure vs. Burnup..... | 58 |
| Figure 9. CCDF for Rod Internal Pressure | 59 |
| Figure 10. Cladding Oxide thickness vs. Burnup Reported by Garde (1991) | 59 |
| Figure 11. PWR Fuel Rod Oxide Thickness for High Burnup Fuels (from Van Swam et al. 1997a)..... | 60 |
| Figure 12. Mean Oxide Thickness and Range vs. Burnup | 60 |
| Figure 13. CCDF for Peak Rod Oxide Thickness | 61 |
| Figure 14. Corrosion: Oxide Thickness vs. Burnup for Alternative Fuel Rod Cladding Materials..... | 61 |
| Figure 15. CCDF for Hydrogen Concentrations in PWR Fuel Rods | 62 |
| Figure 16. Cladding Radial Hydride Profiles (From Schrire et al. 1994) | 62 |
| Figure 17. Crack Size Distribution for PWR Rods | 63 |
| Figure 18. CCDF for Cladding Stress | 63 |
| Figure 19. BWR: Distribution of Failed Rods in WPs..... | 64 |
| Figure 20. PWR: Distribution of Failed Rods in WPs..... | 64 |
| Figure 21. CCDF for Combined BWR & PWR Perforated Rods | 65 |
| Figure 22. Fuel Reliability as a Function of Calendar Year..... | 65 |
| Figure 23. Fuel Rod Reliability Reported by Sanders et al. (1992) | 66 |
| Figure 24. Temperature History Representing Dry Storage and Transportation | 66 |
| Figure 25. Cladding Creep Strain from Dry Storage and Transportation | 67 |
| Figure 26. Details of CCDF for High rod Stress | 67 |
| Figure 27. CCDF for Rod Stress Intensity Factors..... | 68 |

TABLES

| | Page |
|---|------|
| Table 1. DTN Table for Input Data | 9 |
| Table 2. Design Characteristics of Base Case Fuel Assembly..... | 17 |
| Table 3. Observed Fission Gas Releases (Percentages)..... | 20 |
| Table 4. CCDFs for Fission Gas Release vs. Burnup | 23 |
| Table 5. Statistical Summary for FGR Distribution..... | 23 |
| Table 6. Composition of Fission Gas and Half-Lives, Fort Calhoun Fuel Rods..... | 24 |
| Table 7. Effect of Helium Production on Rod Pressure | 25 |
| Table 8. Causes of Fuel Failures in PWRs*..... | 34 |
| Table 9. Fuel Reliability vs Burnup ^a | 36 |
| Table 10. Comparison of Fuel Reliability from Various Sources..... | 38 |
| Table 11. Comparison of Maximum Cladding Design Temperatures for Shipping Casks | 45 |
| Table 12. CCDFs Describing Expected Fuel Stream into YMP | 46 |
| Table 13. Percent and Cause of Rods failed in a WP..... | 46 |
| Table 14. CCDF for Rods with Failed Cladding in a WP..... | 47 |

1. PURPOSE

The purpose of this analysis is to describe the condition of commercial zircaloy clad fuel as it is received at the Yucca Mountain Project (YMP) site. Most commercial nuclear fuel is encased in Zircaloy cladding. This analysis was developed to describe cladding degradation from reactor operation, various degradation modes during reactor operation, and creep during dry storage. Ranges and uncertainties have been defined. This analysis will be the initial boundary condition for the analysis of cladding degradation inside the repository.

2. QUALITY ASSURANCE

This analysis was prepared in accordance with the Civilian Radioactive Waste Management System (CRWMS) Management and Operating Contractor (M&O) Quality Assurance (QA) program. The information provided in this analysis will be used in evaluating the post-closure performance of the Monitored Geologic Repository (MGR) in relation to waste form degradation. The Performance Assessment Operations (PAO) responsible manager has evaluated the technical document development activity.

3. COMPUTER SOFTWARE AND MODEL USAGE

Microsoft Excel for Windows Version 4.0 was used. The analysis was performed on a Dell Pentium personal computer (CPU number 111920) with a WINDOWS 95 operating system. Excel is an industry standard software, and no macros or subroutines were used.

The calculations documented in this report are contained in the Excel file Rod-Initial-C.xls and Fuel-rel.xls. The Excel files are found under the output Data Tracking Number (DTN) number TBD. Parts of this Excel file are included as Attachment II.

4. INPUTS

4.1 DATA AND PARAMETERS

Most of the data used in this analysis is from the published literature for Pressurized Water Reactor (PWR) fuel performance and the respective reference is cited where the data are used. The fuel rod burnup distribution was taken from AP-3.14Q:

Table 1. DTN Table for Input Data

| DTN No. | Data | Source | Where Used in AMR |
|------------------------|--|---|--|
| MO9912SPA FSDR1.002 | W1717 Dimensions, & fill pressure | DOE 1992, P2A-30ACC: WQO.19920827.0001 | Table 2, section 6.3.1 |
| MO9912SPA FGP72.003 | Fission gas production 31 cm ³ /MWd (@ STP) | Rothman p.21, Table 6, References ANS 5.4 (Garde references same #)ACC: NNA.19870903.0039 | |
| MO9912SPA FGR11.004 | Fission Gas Release Fractions | A.M. Garde, 1986 | Figure 4, p.26 |
| MO9912SPA FGR00.005 | Fission Gas Release Fractions | Manzel, R. and Coquerelle, M. 1997TIC: 232556 | Figure 1, p. 465 |
| MO9912SPA FGR00.006 | Fission Gas Release Fractions | Morel, M.; Melin, P.; and Dumont, A. 1994TIC: 243043 | Figures 3 & 4 |
| MO9912SPA FGR00.007 | Fission Gas Release Fractions | Van Swam, L.F.; Strasser, A.A.; Cook, J.D.; and Burger, J.M. 1997TIC: 232556 | Figure 9, p. 459 |
| MO9912SPA FGR00.008 | Fission Gas Release Fractions | Bain, G.M.; McInteer, W.A.; Papazoglou, T.P. 1985TIC: 226810 | Figure 4, p. 4-13 |
| MO9912SPA FGR06.009 | Fission Gas Release Fractions | Guenther, R.J.; Blahnik, D.E.; Campbell, T.K.; Jenquin, U.P.; Mendel, J. 1988bTIC: 223978 | p. 21 high gas release |
| MO9912SPA FGR34.010 | Fission Gas Release Fractions | Lanning, D.D.; Beyer, C.E.; and Painter, C.L. 1997TIC: 238923 | Table 2.2 |
| Applied for | Fission Gas Release Fractions | EPRI (Electric Power Research Institute) 1991TIC: 236839 | Table A1-6, p. A.A-6 |
| MO9912SPA HEL06.012 | He Production | Manaktala, H.K. 1993TIC: 208034 | Figure 3-4, p. 3-12 |
| MO9912SPA FRV23.013 | Free volume | Smith, G.P., Jr.; Pirek, R.C.; Freeburn, H.R.; and Schrire, D. 1994TIC: 245407 | Figure 4.2.4, p. 4-23 |
| MO9912SPA FRT00.014 | Surface oxidation vs. Burnup | Van Swam, L.F.; Strasser, A.A.; Cook, J.D.; and Burger, J.M. 1997aTIC: 232556 | Figure 8 Basis for Surface Corrosion Model |
| MO9912SPA SOX00.015 | Surface oxidation vs. Burnup | Van Swam, L.F.; Strasser, A.A.; Cook, J.D.; and Burger, J.M. 1997aTIC: 232556 | Pilling-Bedworth factor used for cladding loss |
| MO9912SPA HPM34.016 | Hydrogen Absorption Fraction | Lanning, D.D.; Beyer, C.E.; and Painter, C.L. 1997TIC: 238923 | p. 8.4, 8.10 |
| MO9912SPA CSD06.017 | Crack Size Distribution | Sanders, T.L.; Seager, K.D.; Rashid, Y.R.; Barret, P.R.; Malinauskas, A.P.; Einziger, R.E.; Jordan, H.; Duffey, T.A.; Sutherland, S.H.; and Reardon, P.C. 1992TIC: 232162 | p. I-52, III-60 |
| MO9912SPA CDD06.018 | Crack Size Distribution | Sanders, T.L.; Seager, K.D.; Rashid, Y.R.; Barret, P.R.; Malinauskas, A.P.; Einziger, | p. III-56 |

| DTN No. | Data | Source | Where Used in AMR |
|---------------------|--------------------------|---|--|
| | | R.E.; Jordan, H.; Duffey, T.A.; Sutherland, S.H.; and Reardon, P.C. 1992TIC: 232162 | |
| MO9912SPA ROD00.019 | Rod Failure Data | Yang, R.L. 1997TIC: 232556 | Table 1 PWR & BWR Data 1989 to 1995 Frequencies & types of failures, # assemblies discharged |
| MO9912SPA FFD37.021 | Rod Failure Data | EPRI (Electric Power Research Institute) 1997 (Jones)TIC: 236839 | Average of 2.2 rods failed/failed assembly |
| MO9912SPA ASF01.020 | Rod Failure Data | DOE (EIA), 1996TIC: 232923 | Table 5, p. 21 Assemblies discharged 1969 – 1988 |
| MO9912SPA BWR50.022 | BWR Fuel Reliability | Bailey, W.J. and Wu, S. 1990TIC: 234608 | Table 30, data on p. 69 – 85 |
| MO9912SPA GE800.023 | BWR Fuel Reliability | Potts, G.A. and Proebstle, R.A. 1994TIC: 243043 | Table 2, p. 92 1986 – 1988 |
| MO9912SPA CFF00.024 | BWR Fuel Reliability | Yang, R.L. 1997TIC: 232556 | Table 1 |
| MO9912SPA BWRR1.025 | GE BWR fuel Design Data | DOE (U.S. Department of Energy) 1992ACC: HQO.19920827.0001 | p. 2A-15, 2A-21 number of rods in 7x7 and 8x8 assem. |
| MO9912SPA PWR50.026 | PWR Fuel Reliability | Bailey, W.J. and Wu, S. 1990TIC: 234608 | Table 30, data on p. 69 – 85 |
| MO9912SPA PFR01.027 | PWR Fuel Reliability | DOE (EIA), 1996TIC: 232923 | Table 5, p. 21 Assem. discharged |
| MO9912SPA PFR0.028 | PWR Fuel Reliability | Yang, R.L. 1997TIC: 232556 | Table 1 Assemblies discharged and failure rates |
| MO9912SPA FFR76.029 | Dry Storage | McKinnon, M.A. and Doherty, A.L. 1997TIC: 237126 | P. 2.1 & 5.16 Observed failure rate = 0.045% |
| MO9912SPA MCC00.030 | Creep equation | Matsuo 1987, p. 23TIC: 237137 | Creep equation |
| MO9912SPA SFC00.032 | Creep failure criteria | Chung et al. 1987, Table 1,2TIC: 238255 | Failure criteria, 6.10.1 |
| MO9912SPA THD00.031 | Dry Storage Temperatures | Peehs 1998, Fig. 13aTIC: 245171 | Temperature History for Dry Storage Cask |
| Requested | Burnup distribution | AP3.14: APWP99366.Ta | Burnup distrib. 6.2 |

4.2 CRITERIA

No specific criteria were used.

4.3 CODES AND STANDARDS

No specific codes and standards were used.

5. ASSUMPTIONS

5.1 ASSUMPTIONS FOR CLADDING TYPES

The commercial nuclear fuel with stainless steel cladding (1.15% of commercial fuel inventory) is grouped with the inventory of DOE fuels and no credit is taken for the cladding. The basis for this assumption is that fuel with stainless steel cladding represents a very small population of the fuel assemblies to be stored. It also represents a design of cladding that was abandoned in the early years of commercial reactor operation. This assumption is conservative since the stainless steel would be expected to have some reducing affect on dissolution. However, no cladding credit is taken for stainless steel and it is assumed that this fuel is immediately exposed for dissolution when the waste package fails. (See section 6.1) ✓

The Westinghouse 17 by 17 Lopar design (called W1717WL) fuel rod was selected to model all fuel cladding. The basis for this assumption is that this design is the most commonly used element, constituting 21 percent of the discharged Pressurized Water Reactor (PWR) assemblies. The W1717WL is the largest fraction of the more general W1717 type design that constitutes 34 percent of the discharged PWR fuel. The W1717 design is the thinnest zircaloy clad fuel (570 microns cladding thickness). (See section 6.1)

The Boiling Water Reactor (BWR) fuel cladding will be modeled with the W1717WL design base PWR fuel cladding. The basis for this assumption is that BWR fuel rods have a lower pressure than the PWR fuel rods, hence the lower stress. In BWR fuel the pressures are lower than PWRs (1.4 to 2.0 MPa vs. 3.8 to 5.8 MPa). The stresses in BWR cladding are about one third of that in PWR (34 MPa vs. 95 MPa at 325°C). Typical BWR cladding is thicker than PWR cladding (813 microns vs. 570 microns). Most BWR fuel is also enclosed in solid flow channels while the PWR assemblies are an open lattice design. Because the PWR fuel cladding operates under higher stress, is thinner, and is not enclosed in a flow channel, PWR fuel was selected for cladding degradation analysis. For BWR fuel, this is conservative. (See section 6.1) — corrosion?

5.2 ASSUMPTIONS FOR ROD INTERNAL PRESSURE

Fission gas production is linearly proportional to the fuel burnup. The basis for this assumption is that Rothman (1984, p.21, Table 6) found the correlation of 31 cm³/MWd (at STP) for the production of fission gas. This is for volumes at standard temperature and pressure. (See section 6.3.2)

The Complimentary Cumulative Distribution Function (CCDF) for the fraction of fission gas released from the fuel structure into the rod free volume can be estimated by fitting a CCDF to observed fission gas releases under various experimental conditions and burnups. This is further discussed in Section 6.3.3.

Most of the fission gas that is produced in the fuel rod is held in the fuel matrix and is not available to pressurize the cladding. The basis for this assumption is that the pressures seen in reports cited in section 6.3.3 show that the actual pressure is very small compared to the pressure expected if all of the fission gases were to be released to the gap and fuel plenum. (See section 6.3.3)

The multiplication factor used to calculate the FGR for the 5% CCDF for all burnup groups is 2.3. The basis for this assumption is that this value is the highest value determined for the ratio of the upper 5% fission gas releases to the median fission gas release calculated in this report. (See section 6.3.3)

There was a 1% chance of having either manufacturing defects, or fuel exposed to repetitive transients, or other unspecified causes that produce FGR 6 times larger than the median values. The bases for this assumption are the observations concluded from a review of the reports of the fuel characterized for YMP testing termed Approved Testing Materials. This is further discussed in Section 6.3.3. ✓

Helium production by alpha decay can be approximated by a correlation given by Manaktala (1993, Figure 3-4, p. 3-12). The basis for this assumption is the corroboration by two other sources. It only becomes important in time periods exceeding 1000 years. (See section 6.3.4)

The helium release fraction is evenly distributed between 50% and 100%. This is conservative because the helium is generated when the fuel is cool, and little or none of it would be released. (See section 6.3.4)

The initial fill and fission gas pressures are 4 MPa at 27°C for helium production determination. The basis for this assumption is that the mean rod internal pressure for the average burnup is about 4 MPa as shown on Figure 8. (See section 6.3.4) — sampled OK

After an initial period of operation during which the fuel pellet contracts due to an initial densification, the fuel pellet will swell linearly with burnup. The basis for this assumption is that the change in free volume as a function of burnup is linear shown on Figure 7, taken from Smith et al. (1994, p. 4-23, Figure 4.2.4). (See section 6.3.5) — check shape does not change?

All cladding behaves as PWR cladding. The basis for this assumption is that the BWR cladding has much lower stresses. Therefore it is conservative to assume that all of the cladding stored in the repository will behave at least as well as the PWR fuel cladding. (See section 6.3.6)

5.3 ASSUMPTIONS FOR SURFACE CORROSION

The corrosion rate is uniformly sampled inside the range of $\pm 28\mu\text{m}$ from the peak oxide thickness for the power histories of P5a, P5b, and P7 taken from Van Swam et al. (1997a, p. 459). The basis for this assumption is that this value ($\pm 28\mu\text{m}$) bounds the data as shown on Figure 12. (See section 6.4)

The amount of metal loss from the cladding is 57% of the thickness of the oxide layer. The basis for this assumption is the reduced density of ZrO_2 and the voids in the oxide layer. This is the inverse of the Pilling-Bedworth factor of 1.75 given by Van Swam et al. (1997b, p. 426). Calculations of volume changes support this value. (See section 6.4)

5.4 ASSUMPTIONS FOR CRACK SIZE DISTRIBUTION

The sharp-tipped crack is the limiting case for evaluating the Delayed Hydride Cracking. The shape and depth of the crack determine the stress intensity at the crack tip. The sharp-tipped crack presents the highest stress at the tip of the crack making this the limiting case. (See section 6.6)

The crack size distribution is exponentially shaped. (See section 6.6)

The 245 fuel assembly failures (of the 485 total failures) were all caused by initial cladding cracks in the rods. The basis for this assumption is that 240 fuel assembly failures were caused by external mechanical events (handling, debris and grid fretting) and no other explanation is available for the remaining 245 failures cited by Yang, (1997, p. 10, Table 1). (See section 6.6)

The cracks in the 245 fuel assemblies cited by Yang (1997, p.10, Table 1) were at least 28% through wall or approximately 163.6 μm . Therefore, it is assumed that these 245 failed fuel assemblies have initial cladding cracks of 160 μm . (See section 6.6)

Each failed fuel assembly has an average of 221 rods and has 2.2 failed fuel rods. The basis for the assumption of an average 221 rods per fuel assembly is the data shown in Attachment 2, page 4. The most common fuel designs are listed along with the number of rods per assembly for each design and the number of fuel assemblies for each designed that have been discharged from commercial reactors. The basis for the average of 2.2 failed fuel rods per assembly is the report by EPRI (1997, p.4-1). This failure value applies for the early years and the number of failed rods per failed assembly has decreased to be closer to one (1) today. The use of the conversion factor of 2.2 rods/assembly for each year over-predicts the rod failure rate in later years. (See sections 6.6, 6.8.1 and 6.8.5)

5.5 ASSUMPTIONS FOR ROD FAILURE DURING REACTOR OPERATION

Fuel will be loaded into waste packages in chronological order that it was discharged from the reactors. This assumption places the fuel from periods with poor fuel performance into the same waste package and therefore increases the range for rod failure probabilities inside the waste package. This assumption also produces a spread in the distribution of the failures in the waste packages over time. The fuel reliability can then be shown as a function of calendar years. (See section 6.8 and section 6.8.5)

No blending of fuel assemblies occurs during loading and the fuel assemblies are loaded into waste package in chronological order of discharge. Those people concerned with even thermal loads of the WPs may consider blending older and cooler fuel assemblies with newer and hotter

fuel assemblies. For the calculation of rod failure distribution, however, it is assumed that no such blending occurs. (See section 6.8)

BWR fuel assemblies had 49 rods per assembly in the period of 1969 through 1976. This assumption is based on the fact that the early design was a 7 x 7 array with 49 fuel rods in the array. Although the newer 8 x 8 design was beginning to be introduced late in this period, the number of assemblies is insignificant. (See section 6.8.1)

BWR fuel assemblies had an average of 56 rods per assembly in the period between 1977 and 1980. The basis for this assumption is that it is assumed that half of the assemblies during this period were the new 8 x 8 design (62 rods per fuel assembly) and half were the older 7 x 7 design (49 rods per assembly). (See section 6.8.1)

To estimate the range of failed rods in a waste package (WP), it is assumed that each year's discharged fuel assemblies were placed, chronologically, into waste packages. This means that blending does not occur and the period of high rod failures produces waste packages with higher failure rates than the average. (See sections 6.8.1 and 6.8.2)

Fifty percent (50%) of the failed rods have adjacent rods with incipient failures, and that the total failure distributions are increased by approximately 16.5% (0.33×0.50). The basis for this assumption is that Yang shows a failure of 33% and an interpretation of McDonald and Kaiser's data shows a 50% chance of the debris causing the failure. Yang (1997, Tables 1 and 2, page 10) shows that debris fretting was the cause of failure in 33% of the damaged assemblies. McDonald and Kaiser (1985, Figure 2, p. 2-15) shows the location of 82 rods in a core that were damaged during reactor operation and after steam generator replacement. This could be interpreted as an approximately 50% chance that the debris is of sufficient size or in a specific location to damage adjacent rods. This assumption is quite conservative. (See section 6.8.3)

5.6 ASSUMPTIONS FOR ROD FAILURE DURING DRY STORAGE

If $K_I > K_{IH}$, then the crack will start to propagate and, it is assumed, because of long repository times, failure will occur. K_{IH} is the critical stress intensity factor and K_I is the stress intensity factor. (See section 6.10.2)

The temperature of 260°C is used for the analysis of crack size distribution and stress distribution. The basis for this assumption is the degree of plasticity the material exhibits above 260°C. (See section 6.10.2)

5.7 ASSUMPTIONS FOR ROD FAILURE DURING FUEL SHIPMENT

The fuel shipment took three weeks and the temperature was at the peak for that interval. The basis for this assumption is that reasonable shipments across the country should be completed in three weeks and that the temperature is conservatively set at the maximum for the analysis to evaluate the worst case of time at temperature. (See section 6.11)



6. ANALYSIS/MODEL

6.1 CLADDING TYPES

Commercial reactor fuel design has been evolving over the last 30 to 40 years. Eight of the earlier United States (U.S.) reactors used stainless steel cladding, but no operating U.S. reactor currently uses this type of cladding. A total of 723 metric tons of uranium is contained in stainless steel clad fuel, which is approximately 1.15 percent of the estimated 63,000 metric tons of commercial fuel to be placed in the repository. No cladding credit is taken for stainless steel and it is assumed that this fuel is immediately subject to dissolution when the waste package (WP) fails. This fuel is grouped in a DOE fuel type (or class) where no cladding credit is considered.

Zirconium first became available in industrial quantities in 1946 when a commercially viable process to refine it was developed. The metal was first used in the chemical industry for corrosion control applications such as boiling hydrochloric acid (HCl). Because of its high cost (about \$10/lb for commercial grade tubing), its use tends to be limited in most industrial applications.

Zirconium was introduced as a fuel cladding material in the early 1950s because of its high resistance to corrosion in high temperature water, its relatively high mechanical strength and low thermal neutron absorption coefficient. The low thermal neutron capture cross section is about 30 times less than that of stainless steel, which gives zirconium and its alloys an improved neutron efficiency in water reactors. Nuclear grade zirconium differs from commercial grades in that the hafnium, which naturally occurs with zirconium and has a large neutron cross-section, is removed. Using materials with low neutron absorption cross-sections reduces fuel cost because more neutrons are available for neutron fissioning and energy production. The behavior of these materials in reactor operation has been extensively researched. Such work is reported in the proceedings of meetings sponsored by the American Society for Testing and Materials, "Zirconium in the Nuclear Industry." The American Nuclear Society topical meetings, "International Topical Meeting on Light Water Reactor Fuel Performance," also publish the results of this work in its proceedings. Other technical publications are also available on this topic. The main characteristics of zirconium metallurgy come from its high reactivity with oxygen, from the different type of chemical interactions with the alloying elements and from its strongly anisotropic hexagonal crystal structure.

There are two types of light water reactors: Boiling Water Reactors (BWRs) and Pressurized Water Reactors (PWRs). In a BWR, the reactor coolant is permitted to boil in the reactor core and the steam is piped to a steam turbine to make electricity. In a PWR, the reactor coolant is pressurized so that it does not boil and is piped to a steam generator where a second coolant is permitted to boil, generating steam to be piped to the steam turbine. Both types of reactors are fueled by zirconium alloy rods containing pellets of uranium oxide (UO₂) ceramic material.

Two different alloys of zirconium are currently used: Zircaloy-2 and Zircaloy-4. These alloys were developed to reduce the general corrosion rate in water. Zircaloy-2 tends to be used in BWRs and Zircaloy-4 in PWRs. The primary difference in the two alloys is the nickel content (see Table 1). As the length of reactor fuel cycles is extended, advanced alloys are being developed. New alloys such as M4, M5, and ZIRLO have been developed for reduced corrosion and reduced hydrogen pickup. McCoy (CRWMS M&O 1998a, pp. 6-7 to 6-11) summarizes the various fuel element designs that have been used in the United States. The fuel element design integrates the cladding thickness with other features such as cladding material, rod linear power, gas plenum volume, expected burnup, and rod center line temperatures so that desired pressures and stresses are maintained.

For this initial cladding condition analysis, the Westinghouse W1717WL (17 × 17 Lopar) fuel assembly was selected as the design base fuel assembly. This is the most commonly used fuel assembly, constituting 21 percent of the discharged PWR assemblies to date (CRWMS M&O 1998a, Table 4.1.1-1, pp. 6, 7. The W1717WL is the largest fraction of the more general W1717 type design that constitutes 34 percent of the discharged PWR fuel to date. The W1717 design is the thinnest zircaloy clad fuel at 570 microns cladding thickness (CRWMS M&O 1998a, Table 4.1.2-1, pp. 8-11). Table 2 gives typical characteristics of the Westinghouse W1717WL design (DOE 1992, p. 2A-30 for assembly dimensions used in later calculations).

Rothman (1984, pp. 18-20) summarizes internal rod pressures and concludes that measured BWR pressures are lower after irradiation than PWRs (1.4 to 2.0 MPa for BWRs vs. 3.8 to 5.8 MPa for PWRs). Rothman (1984, p. 20) concludes that the stresses in BWR cladding are about one third of that in PWR (34 MPa for BWRs vs. 95 MPa for PWRs at 325°C). Typical BWR cladding is thicker than PWR cladding (813 microns for BWRs (DOE 1992, p. 2A-21) vs. 570 microns for PWRs). Most BWR fuel is also enclosed in solid flow channels while the PWR assemblies are an open lattice design. Because the PWR fuel cladding operates under higher stress, is thinner, and is not enclosed in a flow channel, PWR fuel was selected for the cladding degradation analysis. It is conservatively assumed that all the cladding behaves as the PWR cladding because the BWR cladding is much thicker and experiences lower stresses.

-related to corrosion

Table 2. Design Characteristics of Base Case Fuel Assembly
(Westinghouse W1717WL)

| | | | |
|---------------------------------------|---------------|--|----------------------|
| Cladding OD ^a | 0.950 cm | Irradiation time ^e | 4.5 yrs ^e |
| Cladding thickness ^a | 0.057 cm | Reactor Coolant Pressure ^c | 14-16 MPa |
| Cladding ID ^a | 0.836 cm | Reactor Coolant Temperature ^c | 300-330°C |
| Rod length ^a | 384.96 cm | Clad ID Temperature ^c | 340-370°C |
| Active core length ^a | 365.76 cm | Burnup (mean) ^b | 44 MWd/kgU |
| Plenum length ^a | 16.00 cm | Oxide thickness ^b | 50 μm |
| Plenum volume/Rod ^b | 8.77 cc | Fission Gas Rel. ^b | 2.5% |
| Effective gas volume/Rod ^b | 23.3 cc | Plenum P.(27°C) ^b | 4.4 MPa |
| Active fuel volume/Rod ^b | 200.61 cc | Stress (27°C) ^b | 29 MPa |
| Initial fill pressure ^a | 2.0 - 3.5 MPa | Stress(350°C) ^b | 59 MPa |
| Rods/Assembly ^a | 264 | Fuel Volume/WP ^{b,d} | 1.112 m ³ |

^a DOE (1992, p. 2A-30)

^b From this analysis

^c Pescatore et al. 1990, p. 7

^d 21 PWR assemblies per waste package

^e 18 month cycle, 1/3 core per cycle change-out

6.2 BURNUP

The fuel assembly burnup strongly affects the condition of the cladding. The burnup determines the amount of cladding surface oxidation, fission gas production and release, and fuel pellet swelling and the corresponding free volume reduction. Figure 1 shows the trend for PWR and BWR burnup over the past several decades. It also shows that the PWRs tend to achieve higher burnups. The expected inventory of PWR fuel assemblies was estimated in Ap-314Q: WP-SEV-99233.Ta. This was transmitted as an Excel file named "WP-SEV-99233_TA_CaseA.xls." This file contains an estimate of all the fuel that YMP is expected to receive, including both PWR and BWR fuel types. This file was copied and modified. The resulting file is "WP-BU-A.xls". Both these files are included on the CD Labeled as Attachment I. The working file was first ordered by fuel type (Column J) and the BWR fuel was deleted. The shipments were then ordered by burnup (BU) (Column G) and the number of assemblies (Column D) in each BU grouping was added (Column A). As a check, the sum of the assemblies in the groups is compared to the total number of assemblies (Row 17355, Columns A and C). The resulting distribution is given in Cells Q5 through T19. Figure 2 shows the expected burnup distribution for PWR fuel assemblies, including expected future higher burnup fuels. The practical limit for batch average discharge burnup is approximately 62 MWd/kgU. This is because shipping of UO₂ is limited to 5% enrichment and most fabrication facilities are licensed for no more than that enrichment. There is also a Nuclear Regulatory Commission (NRC) limit for oxide thickness, which limits the residence time in the reactor. The rod fission gas pressures are also limited to slightly above

reactor system pressure to prevent cladding creeping away from the fuel pellets. All of these restrictions mean that the burnup distribution developed in this analysis is not very sensitive to the data presented in AP3.14Q: WP-SEV-99233. This limit on oxide thickness will force fuel vendors to introduce more advanced alloys. With the higher burnups, more of the cladding will be advanced alloys such as M4, M5 and ZIRLO. These have about one half the oxidation rate of Zircaloy-2 (Z-2) or Zircaloy-4 (Z-4) and therefore half the hydrides. Mardon et al. (1997, p. 408, Figure 3) gives a comparison of Zircaloy-4 to M4 and M5. Charquet et al. (1994, p. 80) discusses hydrogen pickup and its dependency on oxidation rate. In the model presented in this section, no effort was made to account for advanced cladding.

Figure 3 gives the Complimentary Cumulative Distribution Function (CCDF) for the burnup distribution used in this analysis. The mean of this distribution is 44.1 MWd/kgU and the median is 44.7 MWd/kgU. The range is from 5 to 73 MWd/kgU.

6.3 ROD INTERNAL PRESSURE

The internal pressure of the rod influences the possibility of rod failure from cladding creep, hydride reorientation, delayed hydride cracking and stress corrosion cracking as each of these failure mechanisms is driven by stress and temperature. The cladding hoop stress is determined by the internal pressure. The internal pressure is determined by the initial fill pressure, fission gas pressure, and, for extended time durations, helium gas pressure from alpha decay. These partial pressures may be summed. The purpose of this section is to establish a mean, median, range, and distribution of internal pressures for later statistical analysis.

6.3.1 Initial Fill Pressure

The objective of this analysis is to estimate a probability distribution for the initial helium fill pressure in a fuel rod. Early in the history of fuel rod development, helium gas was inserted into the fuel rods to improve the heat transfer across the pellet/cladding gap. DOE (1992) gives the fill pressure for many fuel designs. The W1717WL (17x17 Lopar) uses a range of 2 to 3.5 MPa (DOE 1992, p. 2A-30). The Combustion Engineering (CE) C1616C design uses a fill pressure of 2.1 to 3.2 MPa (DOE 1992, p. 2A-13). Pati and Garde (1985, p. 4-28) state that the CE rods for the Calvert Cliffs reactor used initial fill pressures of 3.2 MPa. Manzel and Coquerelle (1997, p. 463) report using 2.25 MPa fill pressure in the Siemens PWR rods. For the analysis presented here, the W1717WL design will be used, and the fill pressure will be assumed to be uniformly distributed between 2 to 3.5 MPa. The fill gas follows the ideal gas law:

$$P_f(i) = P_f(0) * (FVol(0)/FVol(i)) * (T_k(i)/T_k(0)) \quad (\text{Eq. 6.3-1})$$

Where

- $P_f(i)$ = Fill pressure at time i, MPa
- $P_f(0)$ = Initial fill pressure, MPa, uniformly distributed $2 < P_f(0) < 3.5$ MPa
- $FVol(0)$ = Initial free volume, cm^3
- $FVol(i)$ = Free volume at time i, cm^3
- $T_k(0)$ = Initial fill temperature, 300° Kelvin
- $T_k(i)$ = Temperature at time i, Kelvin

6.3.2 Fission Gas Production

The objective of this analysis is to estimate a probability distribution for fission gas pressure in a fuel rod. The fission gas pressure is a combination of the fission gas production rate in the fuel rod, fission gas release rate from the fuel pellets into the "gap" and gas free volume. The production is linearly proportional to the fuel burnup, $31 \text{ cm}^3 \text{ (STP) /MWd}$ (Rothman 1984, p. 21, Table 6). Standard temperature and pressure (STP) are 273°K and 0.1 MPa . The equation to calculate the pressure from fission gas is:

$$P_{fg}(i) = 31 * BU * Mkg * 0.1\text{MPa} * T_k(i) * FGR / (Fvol(i) * 273^\circ\text{K}) \quad (\text{Eq. 6.3-2})$$

Where

- $P_{fg}(i)$ = Fission gas pressure at time i, MPa
- BU = Burnup, MWd/kgU
- Mkg = Mass of U in one rod, 1.76 kg (W1717WL)
- $T_k(i)$ = Temperature at time i, Kelvin
- FGR = Fission gas release fraction, dimensionless (described below)
- FVol(i) = Free volume at time i, cm^3 (see Section 6.3.5)

This equation is used to calculate internal pressure in the fuel rod due to fission gasses in the gap and gas plenum. This is fully developed in Attachment III where this equation used to calculate the fission gas pressure.

6.3.3 Fission Gas Release Fraction

Most of the fission gas that is produced is held in the fuel matrix and is not available to pressurize the cladding. The fraction of gas that is released from the fuel matrix into the "gap" and gas free volume depends on the fuel pellet temperature history. The fuel pellet temperature history is dependent on the reactor design, fuel rod design, burnup, and power history. The fuel rod design is especially dependent on the linear heat generation rate for the fraction of gas that is released. The fraction of the gas that is released that depends on the power history is related to the occurrence of reactor power transients.

A. M. Garde (1986, Figure 4, p. 19, which is reproduced in this analysis as Figure 4) shows the percentage of fission gas release (FGR) for various nuclear power plant sources and PWR designs as a function of burnup. The figure shows that the FGR increases with burnup and has scatter. Rows 1 and 2 of Table 3 give the best estimate and high values for FGR as a function of burnup based on this figure. These FGRs represent various PWR sources and are below 5%. In the same report, Garde (1986, Table 4, p. 19) gives the measured FGR for 12 rods with burnups of approximately 50 MWd/kgU, and these tests averaged 0.94% (Row 3 of Table 3). These rods were an earlier Combustion Engineering 14×14 design with an initial helium fill gas pressure of 2.8 MPa and linear power of 19 kW/m (Garde 1986, p. b-2, c-1).

Table 3. Observed Fission Gas Releases (Percentages)

| Row No. | Fuel Vendor | Reference | Burnup (MWD/kgU) | | | | |
|---------|--------------|---|--------------------------|------------------------|---------|-------|-------|
| | | | 20 | 40 | 50 | 60 | 80 |
| | | | Fission Gas Releases (%) | | | | |
| 1 | CE | Garde (1986, Fig. 4) Best Est. | 0.5 | 0.8 | 1 | 2 | N/A |
| 2 | CE | Garde (1986, Fig.4) High Value | 1 | 3.3 | 3.8 | 4.5 | N/A |
| 3 | CE | Garde (1986, Table 4) Average of 12 measurements | N/A | N/A | 0.94 | N/A | N/A |
| 4 | Siemens | Manzel et al. (1997, Fig. 1) Best Est. | 6 | 6.6 | 7.5 | 8.6 | 14 |
| 5 | Siemens | Manzel et al. (1997) High Value | N/A | 8 | 9 | 10 | N/A |
| 6 | Fragema | Morel (1994, Fig. 4) Best Est. | 0.3 | 0.8 | 1.8 | 3 | N/A |
| 7 | Siemens | Van Swam (1997a, Fig. 9) Best Est. | N/A | 1 | 3 | 4.5 | 8 |
| 8 | Siemens | Van Swam (1997a, Fig. 9 High Value | N/A | N/A | 3.2 | 5 | 9 |
| 9 | B&W | Bain et al. (1985, Fig. 4), Best Est. | N/A | 1.5 | 1.6 | N/A | N/A |
| 10 | B&W | Bain et al. (1985) High Value | N/A | 3.4 | 3.8 | N/A | N/A |
| 11 | N/A | Median for CCDF | 1.69 | 2.14 | 2.98 | 4.53 | 11.00 |
| 12 | N/A | Average High Values | N/A | 4.90 | 4.95 | 6.50 | N/A |
| 13 | N/A | Average High/Median | N/A | 2.29 | 1.64 | 1.44 | N/A |
| 14 | CE | Manaktala (1993, Fig. 3-5) Maine Yankee | 12 to 15 | N/A | N/A | N/A | N/A |
| 15 | Westinghouse | Barner (1985, ATM-101, p. 4.9) (10 rods) | 0.15 to 0.27 | N/A | N/A | N/A | N/A |
| 16 | CE | Guenther (1988a ATM-103, p. 4.15) | 0.25 (@ 30 MWd/kgU) | | N/A | N/A | N/A |
| 17 | CE | Guenther (1991 ATM-104, p. 8.9) (3 rods measured) | N/A | 0.38, 0.62, 1.10 | N/A | N/A | N/A |
| 18 | CE | Guenther (1988b, ATM-106, p.2.1) (3 rods measured) | N/A | 1.4, 7.4, 11.2 | N/A | N/A | N/A |
| 19 | GE | Lanning et al. (1997, Transients, Tbl. 2.1, 2.2) | 3.5-38 | 3.5-44.1 | 13-14.4 | 22-34 | N/A |

Manzel and Coquerelle (1997, pp. 464 and 465, Figure 1) measured FGR for rods with burnups of approximately 80 MWd/kgU (their Figure 1 is reproduced here as Figure 5). These Siemens-designed rods had an initial fill gas pressure of 2.25 MPa. The rods operated at 27 to 31 kW/m in the first cycle (much higher than Garde's rods) and, by the seventh cycle, the rods were operating at 13 to 16 kW/m. The FGR best estimate and high values are summarized in Rows 4 and 5 of Table 3 and are high compared to values reported by others. This could be because of the higher linear power.

Morel et al. (1994, Figure 4, p. 18) reports FGR for fuel of Framatome design that was operated in either regular or load-following (varying power to match demand) generation. Morel et al. show FGR increasing to approximately 3% at burnups of approximately 60 MWd/kgU, results that are similar to that of Garde. Morel's data is summarized on Row 6 and does not give any ranges. Load-following generation is not considered in this analysis as a factor that would tend to increase FGR. Morel et al. (1994, Figure 3, p. 18) also show that fuel rod power spikes rising from a steady state of approximately 15 kW/m to a peak of approximately 25 kW/m increase the

FGR, with about seven power spikes over time subsequently resulting in a total release of approximately 8% FGR with "bursts" evident after each transient.

Van Swam et al. (1997a, p. 459) describe the Siemens high burnup fuel program and, in Figure 9, they give FGRs for fuel approaching 75 MWd/kgU. Their results were extrapolated to 80 MWd/kgU and best estimate and high values are shown on Rows 7 and 8 of Table 3.

Bain et al. (1985, Figure 4, p. 4-13) give FGR including approximate ranges for 32, 40, and 50 MWd/kgU burnups for Babcock and Wilcox (B&W) designed rods. These rods operated at about 15 kW/m. The authors attribute the large FGR ranges to the location of the rod in the assembly and small differences in the rod power histories. Their data were included in Garde's summary (Figure 4 of this analysis) as the Oconee-1 data and are shown in Rows 9 and 10 of Table 3.

The data cited above and summarized in Table 3 represent FGR for five different sources and various burnups. For the purpose of building a CCDF, the best estimates of the reported FGR have been averaged and used as the median (50%) value (see Row 11 of Table 3). These values are conservative because they are high when compared to the release rates reported by U.S. fuel manufacturers (Garde for Combustion Engineering fuel, and Bain for Babcock and Wilcox fuel). The median values have been added to Garde's (1986) Figure 4 (also Figure 4 of this analysis) and are well above most of Garde's data. This is because of the high releases reported by Manzel and Coquerelle (1997). The high values were also averaged and were considered the upper 5% values since these values encompass almost all the data (see Figure 4 for the plot of 5% values). The ratio of upper 5% to the median was approximately 2.3 for the 40 MWd/kgU burnup. The 2.3 multiplication factor times the median is conservatively used to calculate the FGR for the 5% CCDF for all burnup groups. The median value for 20 MWd/kgU was calculated by averaging the slopes of the burnup dependencies for Garde (Row 1, 20 and 40 MWd/kgU values) and Manzel and Coquerelle (Row 4, 20 and 40 MWd/kgU values) and calculating the value from the 40 MWd/kgU median value. This procedure was necessary because just averaging values at the 20 MWd/kgU group would have produced FGRs higher than the next burnup group.

More extreme values of the CCDF were generated by evaluating other FGR measurements for off-normal fuel types or fuel exposed to transient tests. Manaktala (1993, Figure 3-5) shows Maine Yankee fuel at approximately 15 MWd/kgU with FGRs in the 12% to 15% range. Rothman (1984, p. 19) notes that this fuel was manufactured with defects, including no helium backfill and low fuel pellet densities. The pellets contracted away from the cladding, producing high fuel temperatures and high FGR. Rothman notes that such fuel constitutes less than 1% of all spent fuel anticipated from all sources.

A group of fuels has been characterized for YMP testing. These fuels, termed Approved Testing Materials (ATMs), are also included in Table 3. Fuels ATM-101 (Barner 1985, p. 4.9, Table 4-10 rods measured), ATM-103 (Guenther et al. 1988a, p. 4.15, 2 rods measured) and ATM-104 (Guenther et al. 1991, p. 8.9, Table 8.7 - 3 rods measured) all show releases in the range reported by Garde (1986). ATM 106 (Guenther et al. 1988b, p. 2.1) showed FGRs measured in 3 rods of 1.4%, 7.4%, and 11.2%, respectively, two of which are much higher than measured in other Combustion Engineering designed fuel rods as reported by Garde. No explanation for these high releases was identified in this review. As noted earlier, Morel et al. (1994, Figure 3, p. 18) report

*NRC
fuel
performance
report*

FGR for power spikes in fuel of Framatome design. They show that power spikes from 15 kW/m to 25 kW/m increased the FGR with about seven power spikes producing a total release of about 8% FGR with bursts after each transient. From these observations, it was assumed that there was a 1% chance of having either manufacturing defects, or fuel exposed to repetitive transients, or other unspecified causes that produce FGRs that would be six times the median values. The factor of six is the multiplier used to bring the median at 40 MWd/kgU to the release observed in the Maine Yankee (12 – 15%) (approximately 13%) and ATM-106 (11.6%). For the 1% CCDF for the FGR, the median values of the gas release fractions are multiplied by a factor of 6 for all burnup groups. For lower burnup fuels, this results in FGRs in approximately the 10.1% to 17.9% range. At a burnup of 80 MWd/kgU, the releases were limited to 50%, a limit above the highest observed releases in tests discussed in the next paragraph.

The statistical tail of the CCDF represents fuel that was exposed to transients more severe than those considered in Morel et al. (1994, page 18, Figure 3) but not so severe as to disrupt the core (cause fuel rod failure). Lanning et al. (1997, Table 2.2) show FGR from 3.5% to 44.1% for power transients. The results, summarized in Row 19 of Table 3, show little burnup dependency. At a burnup of 50 MWd/kgU, the ratio of the median to the higher release reported by Lanning is 15. Therefore, the median FGRs for each burnup class were increased by a factor of 15 to represent this CCDF class. The CCDF of 0.22% represents the sum of initiating event frequencies given by for the McGuire Nuclear Station Probabilistic Risk Assessment (PRA) for large break Loss of Coolant Accident (LOCA, LL event) and steam line breaks (T6 event) (Duke Power 1997, pp. 3-6, 3-7). Fission Gas Release for probabilities less than 0.22% were set to the value of 0.22%. Table 4 gives the CCDFs for fission gas release percent for various burnups. The FGRs were limited to 50%, which is approximately 6% higher than measured releases in transient tests reported in Table 3. Since the higher releases are of interest in this analysis, the lower half of the CCDF was set by Garde's releases. The first column of Table 4 gives the CCDF in terms of percent. The second column gives the multiplication factor, which is applied to the median values to produce the other values in the table. When performing calculations for a rod with a specified burnup, the median FGR is calculated by linear interpolation of the median FGRs in Table 4. The distribution is then calculated by selecting a random number between 0 and 100 (CCDF value) and calculating a FGR multiplier by linear interpolation on the column labeled "FGR Multiplier" in Table 4. This multiplier is applied to the median value to obtain the FGR for the rod with the specified burnup.

Table 4. CCDFs for Fission Gas Release vs. Burnup

| CCDF | FGR Multiplier | Burnup (MWd/kgU) | | | | |
|-------------------------|----------------|------------------|-------|-------|-------|-------|
| | | 2-20 | 40 | 50 | 60 | 80 |
| Fission Gas Release (%) | | | | | | |
| 100 | 0.4 | 0.68 | 0.86 | 1.19 | 1.81 | 4.40 |
| 50 (median) | 1 | 1.69 | 2.14 | 2.98 | 4.53 | 11.00 |
| 5 | 2.3 | 3.89 | 4.92 | 6.85 | 10.41 | 25.30 |
| 1 | 6 | 10.14 | 12.84 | 17.88 | 27.15 | 50.00 |
| 0.22 | 15 | 25.35 | 32.10 | 44.70 | 50.00 | 50.00 |
| 0 | 15 | 25.35 | 32.10 | 44.70 | 50.00 | 50.00 |

When the FGR model is integrated with the burnup distribution described in Section 6.2, the resulting FGR distribution as described in Table 5 is generated. The distribution is slightly skewed to the higher FGRs with the mean FGR higher than the median.

Table 5. Statistical Summary for FGR Distribution

| Measure | Value |
|-------------------------|--------------|
| Mean | 4.236 |
| Standard Error | 0.1003 |
| Median | 3.1096 |
| Standard Deviation | 4.490 |
| Sample Variance | 20.157 |
| Kurtosis | 30.82 |
| Skewness | 4.621 |
| Range | 49.269 |
| Minimum | 0.7313 |
| Maximum | 50 |
| 5% - 95% Range | 1.11 - 10.78 |
| Count | 2003 |
| Confidence Level(95.0%) | 0.1967 |

Fission gas inventory is expected to stay constant with time in the repository. Peehs (1998, pp. 4 and 5) demonstrates that the fission gas release rate is near zero at repository temperatures because the diffusion coefficients become small. Using the equation presented in Lanning et al. (1997, p. A.4) that is applicable for temperatures of 27°C (300°K), the diffusion coefficient is approximately 3×10^{-31} m²/sec at room temperature, suggesting little diffusion during most repository times.

The quantity of fission gas will not decrease significantly from nuclear decay. Garde (1986, Table 6, p. 21) gives the composition of krypton (Kr) and xenon (Xe) fission gas release as element volume percentages for Fort Calhoun rods. Garde (1986, Table 6, p. 21) gives these

element volume percentages of the components and their respective half lives (Lide and Frederikse 1997, CRC Handbook of Chemistry and Physics, pp. 11-58 to 11-59 and 11-84 through 11-86. The table shows that only about 5% of the Krypton will decay.

Table 6. Composition of Fission Gas and Half-Lives, Fort Calhoun Fuel Rods

| Fission Gas Isotope | Element Volume % ^a | Half Life, Years |
|---------------------|-------------------------------|------------------|
| Kr83 | 9.22 | Stable |
| Kr84 | 35.48 | Stable |
| Kr85 | 4.61 | 10 |
| Kr86 | 50.69 | Stable |
| Xe130 | 0.22 | Stable |
| Xe131 | 5.69 | Stable |
| Xe132 | 23.97 | Stable |
| Xe134 | 27.76 | Stable |
| Xe136 | 42.36 | Stable |

^a Rod KJE006 values reported as representative.

6.3.4 Helium Production

Both Delayed Hydride Cracking (DHC) and strain failures are driven by the cladding stress which may be caused by the internal gas (including initial fill gas, fission product gases, and helium gas from alpha (α) decay) pressure buildup. The gas pressure will slowly increase over time by the production of helium (He) which is produced in nuclear decay as an alpha particle. Manaktala (1993, Figure 3-4, p. 3-12) presents the helium pressure buildup for 100°C as a function of time for a PWR fuel rod with 36 MWd/kgU burnup and an assumed 100% helium release. That figure has been reproduced as Figure 6 and two straight line fits were included. The pressure change profile (after adjustment for temperature) is used in this analysis. The pressure change curve (in log-log space) was approximated by two linear equations, one for less than or equal to 1,000 years and one for above that time.

$$\begin{aligned}
 P_{\text{He}}(\text{MPa}) &= 0.019953 * t^{0.65} && \text{For times, } t \leq 1,000 \text{ years:} \\
 P_{\text{He}}(\text{MPa}) &= 0.17783 * t^{0.3333} && \text{For time, } t > 1,000 \text{ years:}
 \end{aligned}
 \tag{Eq. 6.3-3}$$

where P_{He} = pressure, MPa, at 100°C and the release fraction = 1.0 (i.e., 100% He release)

Table 7, taken from Smith et al. (1994, p. 4-23, Figure 4.2.4), gives the temperature and pressure history for a typical rod in the repository. For periods of high temperatures, such as during the first 100 years, the helium will contribute approximately 7% of the total pressure. This table represents an upper limit since it assumes 100% helium release. As noted in the previous section, the diffusion coefficients for fission gasses become very small at lower temperatures and 100% helium release is unlikely. For this analysis, the helium release fraction will be assumed evenly distributed between 50% and 100%. This is conservative because little or none of the helium generated when the fuel is cool would be released. The correlation was developed for a burnup of 36 MWd/kgU and is adjusted for other burnups assuming a linear correlation.

The final equations are:

$$P_{\text{He}}(\text{MPa}) = 1.4859\text{E-}6 * \text{BU} * T_k * \text{HGR} * t^{0.65} \quad t \leq 1,000 \text{ years:} \quad (\text{Eq. 6.3-4})$$

$$P_{\text{He}}(\text{MPa}) = 1.3243\text{E-}5 * \text{BU} * T_k * \text{HGR} * t^{0.3333} \quad t > 1,000 \text{ years:}$$

Where

- P_{He} = pressure, MPa,
- Bu = Burnup, MWd/kgU
- T_k = Temperature, Kelvin
- HGR = Helium release fraction, uniformly distributed, $0.5 < \text{HGR} < 1.0$
- t = Time from reactor discharge, years

Table 7. Effect of Helium Production on Rod Pressure

| Time (yrs) | Temperature (°C) | Helium Pressure (MPa) | Fission Gas Pressure (MPa) ^a | Total Pressure (MPa) | He % of total Pres. |
|------------|------------------|-----------------------|---|----------------------|---------------------|
| 1 | 210 | 0.03 | 6.44 | 6.5 | 0.40 |
| 10 | 240 | 0.12 | 6.84 | 7.0 | 1.76 |
| 100 | 150 | 0.45 | 5.64 | 6.1 | 7.41 |
| 1,000 | 104 | 1.80 | 5.03 | 6.8 | 26.34 |
| 10,000 | 79 | 3.62 | 4.69 | 8.3 | 43.51 |
| 100,000 | 27 | 6.64 | 4.00 | 10.6 | 62.40 |
| 1,000,000 | 27 | 14.30 | 4.00 | 18.3 | 78.15 |

a: Initial fill and fission gas pressure assumed to be 4 MPa at 27°C. →

For corroborating data, Rothman (1984, p. 21, Table 6) also considered helium production in a Calvert Cliffs reactor PWR rod with a burnup of 36 MWd/kgU. This helium source term was evaluated to produce a helium partial pressure of 3.7 MPa at 10,000 years, very close to the 3.6 MPa using Manaktala (1993) and calculated above. Berggren (1980, p. 4) predicts approximately 15 MPa of helium pressure in one million years for a BWR rod assuming 100% helium release. This is in good agreement with the estimate in Table 7.

6.3.5 Free Gas Volume

The free gas volume is the plenum volume plus the volumes in the rod available for the fission gas and helium to occupy. This volume decreases with burnup. Figure 7, taken from Smith et al. (1994, p. 4-23, Figure 4.2.4), shows the change in free volume as a function of burnup. An

initial positive change (i.e., free gas volume increase) is also reported by Lanning et al. (1997 Figure 4.4, p. 4.4) and is attributed to an initial pellet densification. After this initial period of pellet contraction (densification), the pellet swelling is linear with burnup. The free volume decrease was estimated by Smith et al. (1994) by the equation but with uncertainty added:

$$FVol = FVol_0 - [Unc * (0.15 * BU - 1.0)] \quad (Eq. 6.3-5)$$

Where

| | | |
|-------------------|---|---|
| FVol | = | Free volume, cm ³ |
| FVol ₀ | = | Initial free volume, cm ³ |
| Unc | = | Uncertainty distribution, uniform from 0.75 to 1.25 |
| BU | = | Burnup, MWd/kgU |

The uncertainty distribution was selected to cover the range observed from various designs shown in Figure 7 at a burnup of approximately 58 MWd/kgU. It was introduced as a multiplication term so that it approaches zero as the volume change approaches zero. A uniform distribution was used.

The free volume for the W1717WL (or Lopar) design was estimated based on the dimensions of the W1717WL (DOE 1992, p. 2A-30) to be 23.3 cm³. This free volume decreases with burnup based on Equation 6.3-5.

6.3.6 Plenum Pressure Distribution

Having generated correlations for fill pressure (Equation 6.3-1), fission gas pressure (Equation 6.3-2), helium pressure (Equation 6.3-4), and gas free volume (Equation 6.3-5), a probability distribution for the plenum pressure buildup can now be generated. Figure 8 shows the fuel rod internal pressure as a function of burnup. This curve is for 27°C and helium buildup for 100 years. Also shown are the minimum and maximum pressures after 2000 statistical samplings. The mean pressures are consistent with or slightly higher than reported measurements. Einziger et al. (1982, p. 66, Section II.C) measured pressures of 2.28 and 2.8 MPa after 2 cycles. Garde (1986, Table 7, p.28) reported pressures for 12 fuel rods in the range of 3.51 to 4.04 MPa with a mean of 3.80 MPa, for rods with a burnup in the range of 50-56 MWd/kgU. Figure 8 shows a mean pressure of 5 MPa at 50 MWd/kgU, slightly higher than Garde's measurement because of the higher fission gas release predicted including the data from Manzel et al. (1997). *other temps?*

A desirable upper limit for plenum pressure at end of life is the pressure that exceeds the reactor system pressure (about 15 MPa at 320°C or 7.5 MPa at 27°C). High burnup designs are starting to approach internal pressures that slightly exceed reactor system pressure but are sufficiently low as to ensure that the cladding does not creep away from the pellets (lift-off) during reactor operation. Figure 8 shows that the mean rod internal pressure approaches reactor system pressure at about 65 MWd/kgU at 25°C (pressure 7.5 MPa). Rothman (1984, pp. 18-20) summarizes end of life rod pressures and concludes that pressures at 25°C in PWR fuel rods of 3.8 to 5.8 MPa are typical and maximum values of 7.7 to 8.3 are rare. He also notes that measured BWR pressures are lower, 1.4 to 2.0 MPa, and concludes (Rothman 1984, p.20) that the stresses in BWR cladding at the end of reactor life are about one third of that in PWR ✓

cladding (34 MPa vs. 95 MPa at 325°C). It is conservatively assumed in this calculation that all the cladding behaves as the PWR cladding because the BWR cladding has much lower stresses. *different materials*

The rod pressurization model is integrated with the expected burnup distribution model summarized in Section 6.2 to produce a rod internal pressure CCDF, Figure 9. Again, this CCDF is for 27°C and helium inventory for 100 years of alpha decay. The mean pressure is 4.8 MPa and the median is 4.5 MPa. The range is 2.1 MPa to 17.6 MPa. The 5% - 95% range is 3.0 MPa to 7.3 MPa. Approximately 4.5% of the rods have internal pressure approaching the reactor system pressure (7.5 MPa at 27°C, 15 MPa at a reactor temperature of approximately 320°C).

6.4 SURFACE CORROSION

As the fuel is irradiated in the reactor, the outer surface oxidizes, thus thinning the cladding and producing hydrogen, some of which is absorbed into the cladding. Figure 10, taken from Garde, (1991, p. 583) shows the maximum oxide thickness increases as a function of rod average burnup for CE fuel. The oxide thickness is at a maximum near the upper end of the fuel rod where there are both high coolant temperatures and high linear powers. The figure also shows the scatter in the data. Figure 11, taken from Van Swam et al. (1997a, p. 459), shows the peak oxide thickness for burnups up to approximately 75 MWd/kgU and shows ranges for the data. The authors (i.e., Van Swam et al. (1997a)) suggest linear fits intersecting at 37 MWd/kgU with two different equations for two different power histories. An oxide thickness model was developed using the power history P5a (denoting the higher linear generation rate) of Figure 11. This data was fitted with two linear equations:

$$\begin{aligned} \text{Ox } (\mu\text{m}) &= 0.81081 \cdot \text{Bu} + \text{Unc.}, \text{ for Bu } \leq 37 \text{ MWd/kgU} & (\text{Eq. 6.4-1}) \\ \text{Ox } (\mu\text{m}) &= 2.7907 \cdot \text{Bu} - 73.256 + \text{Unc.}, \text{ for Bu } > 37 \text{ MWd/kgU} \end{aligned}$$

Where

- Ox = oxide thickness in μm , $\leq 120 \mu\text{m}$
- Bu = burnup, in MWd/kgU
- Unc. = Uncertainty Range, = -28 μm to +28 μm , uniformly distributed

Figure 12 shows the corrosion model with the ranges of plus or minus 28 microns above or below the median values. This range captures most of the scatter for each of the three (3) power histories (P5a, P5b, and P7). The lower oxide thickness observed in the P7 power history at 70 MWd/kgU has been neglected since it represents a minimum corrosion rate. It was assumed that the corrosion rate was uniformly sampled inside that range. The corrosion was limited to 120 microns. This is 20 microns above an NRC limit of 100 microns (Essig 1999, Enclosure 1, p. 2) for normal operation and Anticipated Operational Occurrences (AOOs), transients that might occur at least once in the plant lifetime. When this corrosion model is integrated with the burnup distribution given in Section 6.2, the CCDF shown in Figure 13 is generated. Some of the statistical results of this model are:

| | |
|-------------------------------|---|
| Mean cladding thickness: | 54.2 μm |
| Median thickness: | 52.0 μm |
| 5% - 95% range: | 5.28 μm to 112 μm |
| % at 120 μm limit: | 2.55% |

Equation 6.4-1 gives the oxide thickness on the cladding for various burnups. Cladding metal loss is approximately 57 percent of the oxide thickness because of the reduced density and voids in the zirconium oxide (ZrO_2). This percent of the oxide thickness is the inverse of the Pilling-Bedworth factor of 1.75 given by Van Swam et al. (1997b, p. 426). Calculations, found in this AMR (DTN TBD file rod-initial-c.xls, sheet = "corrosion," cells = "G11 through L15"), of volume changes support this number.

As noted above, the model restricted the cladding oxide thickness to 120 microns, 20 microns above the current NRC limit. Figure 14 (Wilson et al. 1997, p.28, Figure 8) shows the evolution of Westinghouse cladding to ZIRLO to stay below such limits. Framatome has developed M4 and M5 cladding with approximately one half the corrosion rate of the standard Zircaloy-4 (Mardon et al. 1997, p. 407, Figure 1).

6.5 HYDRIDE FORMATION

As the cladding oxidizes, hydrogen is absorbed and forms hydrides in the cladding. The hydride content affects the material properties of the cladding and contributes to the potential for delayed hydride cracking and cladding embrittlement. Charquet et al. (1994, p. 80) show that the amount of hydrides in the fuel cladding depends on the amount of oxidation of the cladding. Cladding oxidation is discussed in Section 6.4. As the cladding oxidizes, the water is the source of the oxygen and hydrogen is released through the chemical reaction: $\text{Zr} + 2\text{H}_2\text{O} \Rightarrow \text{ZrO}_2 + 4\text{H}$. For each mole of zirconium consumed, four moles of hydrogen are produced. Some of this hydrogen is absorbed in the cladding. Lanning et al. (1997) recommend a value of 15% for the hydrogen absorption fraction for the NRCs FRAPCON-3 fuel performance code. This value is based on experimental observations shown in Figure 8.2 of Lanning et al. (1997, p. 8.4 and p.8.10).

Figure 13 gives the percentage of rods that have a peak oxide thickness greater than some value for the rod burnup distribution in Section 6.2. The location of the peak oxide thickness is typically near the top of the core where the coolant temperature and cladding outer surface temperature are at the maximum value. Figure 15 gives the CCDF for the average hydrogen concentration at the point or location of the peak cladding oxide thickness. The mean value is 358 ppm and the median value is approximately 343 ppm with a 95% to 5% range of 34.9 ppm to 738 ppm. These values represent averages across the cladding. The hydrogen content is highest at the outer surface and decreases toward the center. Figure 16, reproduced from Schrire and Pearce (1994, p. 107), gives the normalized distribution of hydrogen across the cladding, including a profile for the location of peak oxide thickness. This figure shows that most of the hydrides are in the outer 100 microns of cladding. The hydrogen content is near its minimum on the inside surface, where cracks exist from pellet cladding interaction.

This analysis is for today's most commonly used cladding material in PWRs, Zircaloy-4. Zircaloy-2 and Zircaloy-4 are very similar. Today's advanced fuels are being discharged with burnups of 45 - 50 MWd/kgU, with a few test assemblies being discharged as high as 60 MWd/kgU. As higher burnup fuels are developed, designers will be forced to use special alloys such as ZIRLO, M4 or M5. Figure 14 demonstrates that these types of alloys would be expected to reduce the degree of cladding oxidation and therefore, also reduce the amount of hydrogen in the cladding.

6.6 CRACK SIZE DISTRIBUTION

Delayed Hydride Cracking (DHC) starts with an existing crack. The shape and depth of the crack determine the stress intensity factor at the crack tip. For this analysis, a sharp-tipped crack shape is assumed as the limiting case. Sanders et al. (1992, p. III-56) present a method for developing a crack-size distribution and recommends a maximum initial crack size for fuel that has not failed during reactor operation to be 28 percent of original cladding thickness. This is based on two different analyses (Sanders et al. 1992, p. I-52 and p. III-60). Cladding with larger initial cracks would be expected to fail during reactor operation as the cracks propagate through the cladding. This analysis uses both Sanders' methodology and maximum crack size. It is assumed that the crack size distribution is exponentially shaped:

$$P(w) = B e^{-Bw} \quad (\text{Eq. 6.6-1})$$

Where

$P(w)$ = probability of having a crack of depth w in a rod
 w = crack depth, μm
 B = constant, $0.0550 \mu\text{m}^{-1}$

This equation is integrated for crack depth from w to ∞ , giving the probability of having a crack of depth w or larger:

$$F(w) = e^{-Bw} \quad (\text{Eq. 6.6-2})$$

Where

$F(w)$ = probability of having a crack of depth w or larger
 w = crack depth, μm
 B = constant, $0.0550 \mu\text{m}^{-1}$

The variable B can be evaluated by reviewing fuel performance and calculating the probability of rod failure from cracks. Yang (1997, p. 10, Table 1) reviewed PWR fuel performance and reported 485 fuel assembly failures in 16,153 assemblies over the period 1991 through 1995, the last five (5) years for which data are available (the table has been reproduced as Table 8 and is discussed in Section 6.8.2). Yang reports the causes of the failures and reports that 240 fuel assembly failures were caused by external events (handling, debris, and grid fretting). It is

assumed that the remaining failures (245) were all caused by initial cladding cracks in rods that were at least 28 percent through wall (approximately 160 μm for the W1717WL). This assumption is conservative, since some if not most of these failures were not caused by cracks. Considering the mixture of the different types of PWR assemblies, an average assembly has 221 rods. It is also assumed that each failed assembly has 2.2 failed rods (EPRI 1997, p. 4-1). The probability of having a crack equal to or greater than 160 μm is:

$$F(160 \mu\text{m}) = 2.2 * 245 / (221 * 16153) = 1.51\text{E-}4 = e^{-B * 160} \quad (\text{Eq. 6.6-3})$$

This equation is used to evaluate B ($B = 0.0550 \mu\text{m}^{-1}$). Figure 17 gives the crack size distribution for PWR rods based on recent fuel failure rates as discussed above. The analytical median (50 percent) crack is about 12.6 μm (2.2% of clad thickness) deep. A maximum crack size for fuel not failing during irradiation is calculated to be 28 percent (160 μm) of cladding thickness (Sanders et al. 1992, p. I-52) and has a probability of 1.51E-4 per rod. The mean crack is approximately 19 μm deep.

Chung et al. (1987, p. 775) reported 20 experiments where irradiated cladding was exposed to hoop stress until failure. In 11 of the tests, the failures were found to have pseudo-cleavage features associated with failures at cracks from Pellet Clad Interaction (PCI). These tests corroborate the existence of cracks on the inside of the fuel cladding.

when is this inappropriate? (inside outside)

When performing the statistical sampling, Equation 6.6-2 is rearranged to express the crack depth, given a random number between 1 and zero:

$$w(\mu\text{m}) = -\ln(\text{rand}()) / B \quad (\text{Eq. 6.6-4})$$

Where

- w(μm) = crack depth
- rand() = random number between 0 and 1
- B = 0.0550 μm⁻¹

6.7 CLADDING STRESS

The total cladding internal pressure is developed in Section 6.3.6. The loss of cladding thickness from surface corrosion is developed in Section 6.4. The size distribution of the cracks is developed in Section 6.6. Hence, a distribution for the hoop stress in the cladding can be calculated. The thin wall approximation from Roark (1989, p. 519, equation 1c) for hoop stress is used. The equation used is:

$$St = P * ID / [(2 * (Th - Ox - w))] \quad (\text{Eq. 6.7-1})$$

- Where:
- St = cladding stress, MPa
 - P = total rod gas pressure, MPa

hypocritical self

| | | |
|----|---|---------------------------------|
| Th | = | initial cladding thickness, cm |
| Ox | = | Metal loss from oxide layer, cm |
| W | = | crack depth, cm |
| ID | = | cladding inside diameter, cm |

No credit is taken for any structural support nor compression stress from the oxide layer. The thin wall approximation underestimates the stress at the inside of the cladding by 7 percent. When compared with the thick wall approximation from Roark (1989, p. 638, equation 1b), this results in an error that is small compared with the other uncertainties in this analysis. Stress concentration at a crack tip is discussed in Section 6.10.2.

The rod internal pressure and cladding oxide metal loss are functions of burnup. The initial clad thickness is 0.057 cm for a W1717WL design. When integrating the above equation with the burnup distribution discussed in Section 6.2, the CCDF for stress (room temperature, 100 years of alpha decay) is shown in Figure 18. The statistical parameters for the distribution of 2000 samplings are:

mean = 38.4 MPa

median = 35.8 MPa

minimum = 15.6 MPa

95% = 23.2 MPa

5% = 61.8 MPa

maximum = 146 MPa

The long tail in the CCDF is caused by the low probability occurrences of high pressures for the high burnup rods as shown in Figures 8 and 9. Rothman (1984, p. 20) reports a "worst-case" stress of 95 MPa at 325°C (47.5 MPa at 27°C). Because of the higher burnup distribution as described in Section 6.2 and the high fission gas release model developed Section 6.3.3, 17.5% of the rods in this analysis exceed Rothman's "worst case" value.

Pescatore et al. (1990, p.67, Table 9) tabulate both average and maximum hoop stresses for both PWR and BWR fuels from many other sources. For 320°C, Pescatore's average values vary from 24 to 62 MPa and his maximum values are up to 134 MPa. He also notes that rods with maximum stresses represent less than 1 percent of the total rods. He shows that BWR stresses are half that in PWRs, partially explaining the choice of PWR fuel as the limiting type fuel for repository design. ✓

6.8 RODS FAILURES DURING REACTOR OPERATION

The objective of this analysis is to calculate a possible rod failure probability distribution for fuel rods that failed during reactor operation (or that would be incipient failures) that might be contained in a WP. The assumption is that the fuel is loaded into the WP in the chronological order that it was discharged from the reactor. This assumption places the fuel from periods with poor fuel performance into the same WP and therefore increases the range for rod failure probabilities inside the WP. In the mid 1970s, there were years where core designs had poor performance. For example, in 1973 almost 60% of the BWR assemblies that were discharged had some perforated rods in them. These older and cooler assemblies would probably be blended in a WP with newer and hotter assemblies to have a more even thermal load of the WPs. For the calculation of rod failure distribution, it is assumed that no blending occurs and the assemblies are loaded into WPs in chronological order of discharge from the reactors.

6.8.1 BWR Rod Failure Distribution

Page 1 of Attachment 2 gives the historic reliability of BWR fuel. Column A gives the calendar year, and Column B gives the number of discharged assemblies for each year (DOE (EIA) 1996, p.21, Table 5 for 1969 – 1988; and Yang 1997, Table 2, p. 10 for the later years). Column C gives the number of assemblies with damaged rods. The data for 1969 through 1985 is from Bailey and Wu (1990, p. 6.23, Table 30). Assembly failure data from 1986 through 1988 was taken from Potts and Proebstle (1994, Table 2, p. 92). Bailey and Wu's (1990) data was not used during this period because the reported failure rates appeared to be too low, suggesting incomplete data. Data for years 1989 through 1995 is taken from R. Yang (1997, Table 2, p. 10). Column D gives the percent of assemblies that were discharged each year with damaged rods. In 1970, all 29 assemblies that were discharged were reported to have damaged rods. In the period 1973 through 1976, the damaged assemblies peaked at approximately 57% and then decreased to approximately 18%. These were pellet-clad-interaction (PCI) failures and led to design changes. Assembly failure rates dropped off after this period. Column G gives the total number of rods discharged each year, and Column H gives the number of failed rods, assuming 2.2 rods failed per damaged assembly (EPRI 1997, p. 4-1). Column E gives the percent of the total number of assemblies over all years that have failed, with the worst year being 1974 where approximately 1% of the total number was damaged. Columns G and H are individually summed and then the average rod failure rate was determined to be approximately 0.17%. This rod failure rate is higher than reported by EPRI (1997, p. 4-1). This means that the actual ratio of failed rods per failed assembly is less than 2.2. This analysis is therefore considered to be conservative.

For the TSPA, it is desired to know what percent of the rods are defective. The above paragraph discusses assemblies with failed rods. EPRI (1997, p. 4-1) reports that, on average, there are 2.2 rods failed per failed assembly. The BWR fuel assemblies were originally 7 by 7 rod designs with 49 rods per assembly. These were replaced in the period of 1977 through 1980 with 8 × 8 rod designs with 62 rods per assembly. (See Sasaki and Kuwabara (1997, Figure 3, p. 17) for an approximate evolution of BWR design.) DOE (1992, p 2A-15 and 2A-21) gives the number of rods per assembly and the most commonly used design was selected. For this analysis, it is assumed that the assemblies have 49 rods through 1976. In the period 1977 through 1980, it was assumed that half the assemblies are new designs and the average is approximately 56 rods per assembly. Starting in 1981, the assemblies contain 62 rods. This evolution is shown in Column

F. Column I gives the percent of rods that have failed in each calendar year. The worst year was 1970 when approximately 4.5% of the rods discharged were estimated to have failed. In 1973, approximately 2.6% of the rods discharged were estimated to have failed.

To estimate the range of failed rods in a WP, it was assumed that each year's discharged fuel assemblies were placed, chronologically, into WPs. This means that blending does not occur and the period of high rod failure rates (1970, and 1973 through 1976) produces WPs with higher failure rates than the average. Column J gives the number of WPs that contain rods with failure rates given in Column I. Column K gives the percent of all BWR WPs that contain rods with the failure rates in Column I. Columns I and K are reproduced in page 2 of Attachment 2 as Columns A and B but are ordered in ascending order of rod failure rates. A Complementary Cumulative Distribution Function (CCDF) is calculated (Column C) and plotted as Figure 19. This figure shows that the range for rods failed in the BWR WP varies from 0.003% to approximately 4.5% with a median of 0.055% and mean of 0.196%.

6.8.2 PWR Rod Failure Distribution

Page 3 of Attachment 2 contains the calculation of the historic reliability of PWR fuel. The same procedure was used to analyze the PWR data as was used for the BWR data as described above. Column A gives the calendar year, and Column B gives the number of discharged assemblies for each year (DOE (EIA) 1996, Table 5 for 1970 – 1988; and Yang 1997, Table 1, p. 10 for 1989 - 1995). Column C gives the number of assemblies with damaged rods. The data for 1970 through 1985 is from Bailey and Wu (1990, Table 30). The rod failure rate for the period 1986 through 1988 was calculated as an average of the previous and later three years (1983 – 1985, 1989 – 1991). This rate is 0.041% and is larger than the 0.006% reported by Westinghouse for their fuel in 1987 and 1988 (Preble et al. 1993, p. B.5). Bailey and Wu's (1990) data for this interval were not used because the reported failure rates appeared to be too low, suggesting incomplete data. Data for years 1989 through 1995 is taken from Yang (1997, Table 1, p. 10). This table has been reproduced as Table 8 in this report. It gives the various causes of rod failure as a function of calendar year and gives the total number of discharged assemblies. Column D of Attachment 2, p. 3 gives the percent of assemblies that were discharged each year with damaged rods. The worst year was 1972 when approximately 13% of the assemblies were damaged. Column E gives the percent of the total number of assemblies that were discharged, with the worst year being 1989 with 0.43% of the total number being damaged. This column also shows that the PWR fuel reliability is more consistent than the BWR fuel reliability by approximately a factor of two.

how PWR represent BWR

Table 8. Causes of Fuel Failures in PWRs*

| Failure Cause | Number of Assemblies | | | | | | | |
|-------------------------|----------------------|-------------|-------------|-------------|-------------|-------------|-------------|----------------|
| | 1989 | 1990 | 1991 | 1992 | 1993 | 1994 | 1995 | 1996 (Partial) |
| Handling Damage | | 6 | 2 | | | 1 | 1 | 1 |
| Debris | 146 | 11 | 67 | 20 | 13 | 6 | 10 | 1 |
| Baffle Jetting | | | | | | | | |
| Grid Fretting | 14 | 18 | 9 | 33 | 36 | 9 | 33 | 19 |
| Primary Hydriding | | 1 | | 4 | | | | |
| Crudging/Corrosion | | | | | | | 4 | 1 |
| Cladding Creep Collapse | | | | | | | 1 | |
| Other Fabrication | 1 | 15 | 1 | 5 | 3 | 1 | 15 | 3 |
| Other Hydraulic | | | | | 1 | | | |
| Inspected/Unknown | | | | | 36 | 36 | 13 | 2 |
| Uninspected | 43 | 58 | 35 | 61 | 14 | 3 | 12 | 1 |
| Totals | 204 | 109 | 114 | 123 | 103 | 56 | 89 | 27 |
| Total Discharged | 2196 | 3461 | 2937 | 3302 | 3612 | 2636 | 3666 | |

* Source: R.L. Yang (1997)

Column F gives the average number of rods per PWR assembly. This number is calculated on Page 4 of Attachment 2. Almost all of the commercial BWR reactors in the U.S. were designed by General Electric (La Cross was a 48 MW BWR designed by Allis Chalmers), and the evolution of the fuel designs was simpler than that of PWRs. The PWRs were designed by three different reactor vendors, and the fuel varied from Combustion Engineering 14 by 14 designs (164 rods) to Westinghouse 17 by 17 designs (264 rods). The average is based on the most common 6 designs. The number of assemblies discharged is from CRWMS M&O (1998a, Table 4.1.1-1). The number of rods for each design is taken from DOE (1992, pp. 2A-7, 12, 13, 26, 28, and 30). The most common six (6) PWR fuel designs, weighted by the number of assemblies discharged, averaged 221.4 rods per assembly. This number was used in Column F for all years.

Column G gives the total number of rods discharged each year, and Column H gives the number of failed rods assuming that 2.2 rods (EPRI 1997, p. 4-1) fail per failed assembly (Column C). To estimate the range of failed rods in a WP, it was assumed that each year's discharged fuel assemblies were placed, chronologically, into WPs. This means that blending does not occur and the period of high rod failure rates (1972 and 1989) produces WPs with higher rod failure rates than the average. Column I gives the rod failure rate for each year, and Column J gives the number of WPs that are required for the number of assemblies discharged that year. These WPs will have rod failure rates given in Column I. Column K gives the percent of all PWR WPs that contain rods with the failure rates in Column I. Columns I and K are reproduced in Page 2 of Attachment 2 as Columns D and E, but are ordered in ascending order of rod failure rates. A Complementary Cumulative Distribution Function (CCDF) is calculated (Column F) and plotted

as Figure 20. Column F shows the percent of WPs that contain more failed rods than given in Column D. This figure shows that the range for rods failed in the PWR WP varies from 0% to approximately 0.12% with a median of 0.032% and mean of 0.033%. For the PWR WPs, the mean and median are very close suggesting a more normal distribution when compared to the BWR WPs.

6.8.3 Incipient Failures

Incipient failures refer to rods that did not fail in the reactor but are sufficiently damaged such that they would be expected to fail prematurely in the WP. One type of incipient failure is cracks in the cladding that were discussed in Section 6.6. Most causes of rod failure are specific design or operational related problems such as baffle jetting or grid fretting, and tend to occur early in the assembly life. Andrews and Matzie (1985, Table 2, p. 2-42) showed that the rod failure rate decreases with cycle of exposure (see Table 9). This shows that the cladding is not deteriorating significantly and that a large incipient failure rate is not expected. Most fuel today resides in the core for 3 cycles (1/3 core replacement approximately every 18 months). If it is assumed that the incipient failure rate is comparable to a fourth cycle, then the incipient failure rate would be 0.00064%, which is negligible compared to other failure rates. Dry storage conditions are very similar to WP conditions. The Idaho National Engineering and Environmental Laboratory (INEEL) dry storage program results are that the failure rate in dry storage was approximately 0.01% for unconsolidated rods and approximately 0.045% for all rods (McKinnon and Doherty 1997, p. 2.1, 5.16). This further shows that incipient failures are unlikely.

Another way to estimate an incipient failure rate is to consider fretting by debris. McDonald and Kaiser (1985, Figure 2, p. 2-15) show the location of 82 rods in a core that were damaged during reactor operation after a steam generator replacement. These failures were attributed to debris fretting. This type of fretting tends to occur early in the cycle, before the fuel builds up a hard oxide layer. Inspection of the referenced figure shows that 39 failed rods (approximately 50%) are adjacent to other failed rods. This could be interpreted as there is an approximately 50% chance that the debris is of sufficient size or in a specific location to damage adjacent rods. Yang (1997, Tables 1 and 2, page 10) shows that debris fretting was the cause of failure in 33% of the damaged assemblies. This analysis will assume that 50% of the failed rods have adjacent rods with incipient failures, and the total failure distributions are increased by approximately 16.5% ($33\% \times 0.50$). This assumption is quite conservative. As pointed out in the first paragraph of this section, rod failure rates decrease with time and incipient failure rates could be many orders of magnitude smaller.

Table 9. Fuel Reliability vs Burnup ^a

| Cycles of Exposure | 1 | 2 | 3 | 4, 5, 6 | Totals |
|---|---------|---------|---------|----------------------|-----------|
| Range of Assembly Burnup Gwd/Mtu | 0 - 20 | 12 - 32 | 20 - 32 | 32 - 52 | N/A |
| Total Number of Fuel Rods in Burnup Range | 799,500 | 620,100 | 450,100 | 109,000 | 1,978,700 |
| Total Number of Leaking Rods | 140 | 50 | 25 | 0 | 215 |
| Percent of Leaking Rods | 0.0175 | 0.0081 | 0.0056 | 0.00064 ^b | 0.011 |

^a Table reproduced from Andrews and Matzie (1985, Table 2, p. 2-42)

^b Rod failure rate estimated using Chi Squared approximation with zero degrees of freedom.

6.8.4 Combined CCDF

A single CCDF for the number of rods failed in either PWR or BWR WPs may be estimated. The BWR and PWR CCDFs may be combined to give a distribution of rod failures for all WPs. Summing Columns J on pages 1 and 3 of Attachment 2 shows that approximately 60% of the WPs contain PWR fuel and the remaining 40% contain BWR fuel. The single CCDF is generated by summing the two individual CCDFs after weighing by 60% (PWR) and 40% (BWR). The total CCDF was then increased by 16.5% to account for the potential for incipient failures. This calculation is shown on page 2 of Attachment 2 and plotted as Figure 21. The tail of the combined CCDF is dominated by the higher failure rates of the early designed BWR fuels. The median of the combined CCDF is 0.04% and the mean is 0.11%.

6.8.5 Corroborating Data

The objective of this analysis is to estimate the distribution of rods that failed during reactor operation (or that would be incipient failures) that might be contained in a WP. The assumption that produces the spread in the distribution was that the "poorer" fuels of the mid-1970s were placed, chronologically, into a group of WPs. Figure 22 gives the BWR and PWR fuel rod reliability as a function of calendar year based on this analysis. Assembly failure rates were converted to rod failure rates using a conversion of 2.2 failed rods per failed assembly. EPRI (1997, p. 4-1) states that this conversion factor applies for the early years and the number of failed rods per failed assembly has decreased to be closer to one (1) today. The use of the conversion factor of 2.2 failed rods/failed assembly for each year over-predicts the rod failure rate in later years. Manaktala (1993, p.3-3 Figure 3-1) shows the failure at BWR plants with older designed fuel rods peaking at about 2% in the 1970s and then falling off as hydriding and PCI problems were reduced with shaped pellets and cladding design changes. The PWR fuel failures peaked in the early 1970s with five (5) plants having Pellet Cladding Interaction (PCI) failures of approximately 5%. Sanders et al. (1992, Figure I-11, page I-37 and reproduced here as Figure 23) show very similar shapes of the reliability curves of both fuel types to those presented in Figure 22 but with lower peaks for the BWRs in the 1970s. Table 10 compares the rod and assembly failure rates from various sources to this AMR. The table shows that 14 of 16 comparisons of the authors report low fuel failure rates in comparison to this AMR. In most

cases, the analysis presented in this AMR over-predicts the failure rates and therefore is conservative.

Yang et al. (1991, p. 268) report an average of 1.4 failed rods per failed assemblies for PWRs and 1.1 failed rods/failed assembly for BWR for their most recent (1991) review. The use of these lower conversion factors would slightly change the means and medians but would not have an effect on the statistical tail of the CCDF because that is determined by the early fuels for which the conversion of 2.2 rods/assembly applies.

Both Figures 22 and 23 show a strong improvement in fuel performance as a function of calendar year. The PWR industry has been plagued with steam generator problems that require steam generator maintenance at most refuelings. This has put great pressure on the operators to keep the primary system as clean as possible. The BWR design runs primary coolant steam through the steam turbine, so they also are under pressure to keep the primary coolant as clean as possible. Most refueling contracts require fuel manufacturers to replace any failed fuel rods from an assembly that is not fully utilized at the next refueling. The Institute of Nuclear Power Operations (INPO) collects and reports reactor performance in terms of fuel cycle, with or without failed fuel. Rod failures have led to sophisticated detection techniques (Sunderland et al. 1994 p. 73) to detect failed fuel and identify in which fuel cycle it is located. Sayles, et al. (1994, p. 76) describe identifying single failed rods in operating reactors and using the ratio of ^{134}Cs to ^{137}Cs to identify in which fuel cycle the failed rod was located. In most cases, failed fuel rods are removed from the assembly and replaced before the assembly is reinserted.

The above analysis addresses the number of rods that have failed during reactor operation. The degree of rod damage in reactor operation (EPRI 1997, p. 4-2 and 4-3) is:

| | |
|--|---------------|
| Pinhole and through wall hairline cracks | 80% to 90% |
| Intermediate condition | 10% to 20% |
| Severe damage | 0.04% to 0.9% |

This means that for most of the failed fuel, the very limited failure of the cladding will still limit the speed in which the fission products will escape when in the reactor as well as during storage and in the repository.

6.8.6 Future Fuels

As noted above, the trend has been for higher fuel reliability. Most current contracts require the vendors to replace any failed fuel, and this is expensive. There is also a trend to increase burnup. Section 6.2 of this report discusses burnup. Today, because burnup is limited to a batch average discharge burnup of about 62 MWd/kgU for licensing considerations, both material shipping and manufacturing are limited to 5% enriched uranium. The average burnup in future cores might be expected to approach the mid-50s MWd/kgU. The NRC limits oxide thickness to 100 microns (Essig 1999, Encl 1, p.2), which either limits the burnup with standard zircaloy or requires advanced alloys. Vendors have introduced advanced alloys such as ZIRLO (Westinghouse, see Figure 14), M4, and M5 (Framatome). It is expected that fuel reliability will be maintained at current levels because of the introduction of new materials and economic pressures.

Table 10. Comparison of Fuel Reliability from Various Sources

| Fuel | Period | Reference | Failure Rate ^a , % | This AMR % |
|------------------------|---------------------------------|---|-------------------------------|----------------------------|
| BWR | Through 1990 | DOE (1992, p. 2.5-4, Table 2.5.2) | 4.9-(Assembly) | 6.5 |
| W-PWR | Through 1990 | DOE (1992, p. 2.5-5, Table 2.5.3) | 1.6-(Assembly) | 3.5. (all PWR) |
| PWR-all | Through 1990 | DOE (1992, p. 2.5-3, Table 2.5.1) | 4.2-(Assembly) | 3.5 |
| All | 1988 | Bailey & Wu (1990, p. 4.2) | 0.0022 | 0.049 |
| GE-8 x 8 | 1983 | Bailey et al. (1985, p. 1-3) | 0.007 | 0.034 |
| PWR-French | 1979 -1984 1984 | Dehon et al. (1985, p. 2-24) | 0.001 - 0.01 0.005 | 0.006 - 0.048 0.018 |
| BWR-Japan PWR-Japan | To 1997 | Sasaki & Kuwabara (1997, p. 13, 14) | 0.01 0.002 | 0.17 0.033 |
| GE-BWR, 8 x 8 | 4/74 - 8/1993 | Potts & Proebstle (1994, p. 92, Table 1) | 0.016 | 0.4, all BWRs |
| PWR-CE | To 11/1984 | Andrews and Matzie (1985, Table 2, p. 2-42) | 0.011 | 0.027 |
| All | Through 1984 | EPRI (1997, p. 4-1) | 0.02-.07 | 0.14 |
| All | After 1984 | EPRI (1997, p. 4-2) | 0.006-0.03 | 0.036 |
| BWR PWR | To 1986 | Sanders (1992, p. I-36) | 0.15-0.68 0.035-0.44 | 0.06 - 4.4 0.006 - 0.13 |
| PWR- Westinghouse | 1 core, after SG replacement | McDonald and Kaiser (1985, pp. 2-5, 2-15) | 0.26 | Within CCDF 0.004 - 5.3 |
| All | 1969 - 1976 | Manaktala (1993, p. 3-3) | 0.01-2+ | 0.004-5.3 |
| PWR-Mark B-B&W | 1986-1996 | Ravier et al. (1997, p. 34, Fig. 4) | 0 - 0.055 | 0 - 0.127 |

^a Failure Rates are on a rod basis unless noted as assembly-based.

6.9 ROD FAILURE DURING SPENT FUEL POOL STORAGE

After discharge from the reactor, the fuel assemblies are stored in uncovered spent fuel storage pools. An International Atomic Energy Agency (IAEA) survey (IAEA 1988, Table XXVI) reported no evidence of fuel degradation in spent fuel pools and no evidence of further degradation in the spent fuel pool of fuel that had been damaged during reactor operation. The oldest fuel in the survey was Shippingport PWR fuel that has been in wet storage since 1959. Other fuels reported to have had no further degradation during storage have been in wet storage since 1962, 1966, 1968, and the 1970s.

Under the DOE Spent Fuel and Fuel Pool Component Inventory Program, the effect of storing both fuel with intact cladding and fuel with failed cladding has been studied. An international

*Survey
Valid
Examination*

survey of water storage (Johnson et al. 1980, p. iii) reports no cases of fuel cladding degradation during pool storage.

Johnson (1977, p. 20) reports: "Operators at several reactors have discharged, stored, and/or shipped relatively large numbers of Zircaloy-clad fuel that developed defects during reactor exposures (e.g., Ginna, Oyster Creek, Nine Mile Point, and Dresden Units I and II). Several hundred Zircaloy-clad assemblies that developed one or more defects in a reactor are stored in the GE-Morris pool without needing special containment. Detailed analysis of the radioactivity in the pool water indicates that the defects are not releasing significant quantities of radioactivity."

of course in YM

The importance of the spent fuel pool storage experience is that fuel failure or degradation is not expected during pool storage, and the fuel failure rates observed from reactor operation are appropriate for the cladding degradation analysis.

6.10 ROD FAILURE DURING DRY STORAGE

Because some utilities are filling their spent fuel pools, they are starting to build and operate dry storage facilities where the fuel is dried and placed in metal canisters filled with inert gasses.

The DOE has sponsored a Spent Nuclear Fuel Integrity During Dry Storage-Performance Tests Program at the INEEL since 1984 (McKinnon and Doherty 1997, pp. 2.1, 5.16). Approximately 26,500 rods have been studied in various commercial dry storage casks. This program also demonstrates what can be expected to happen to fuel in repository WPs during early storage times when temperatures are elevated. The fill gas has been monitored and few rod failures have been observed during dry storage. During fuel consolidation, approximately 10 rods are believed to have developed small leaks. Consolidation removes the spacers from the assembly and permits two assemblies to be stored in the location of one. Some rods leaked, but the release was over 2 months, a very slow gas release. From the leaking rods, only 0.5 percent of ⁸⁵Kr was released. After shipment to the INEEL, the observed rod failure was similar to that after reactor operation. For the rods that were not consolidated, 2 rods leaked out of 16,700 rods producing a failure probability of 1.2E-4/rod. Overall, including the consolidated rods as dry storage failures, the observed failure rate is 0.045%. This will be added to the creep failures predicted in Section 6.10.1.

Dry storage tests were performed at the Nevada Test Site (Johnson et al. 1987 p. iv) with 17 spent fuel assemblies, each in an individual test. These tests contained 3,468 rods, and cladding temperatures varied from 168°C to 380°C. One of the fuel rods failed during these tests. This assembly was exposed to air at 275°C and had nine thermal cycles during the tests. The estimated hole size was 1 micron. No further degradation was observed in this one failed rod after the initial failure. No visible damage was observed in the other tests.

Accelerated high temperature tests were performed on 15 rods with cladding (Einziger et al. 1982, pp. 65, 69). PWR rods were exposed to temperatures of 482°C, 510°C, and 571°C for up to a year in limited air and inert gas atmospheres. No cladding breaches occurred. The cladding had crept away from the pellets and showed a smoother profile. Strains from 1.7 percent to 7 percent were measured. One rod had a local creep as high as 12 percent. The extended lifetime

is due to significant creep strain of the Zircaloy cladding, which decreases the internal rod pressure. The cladding creep also contributes to radial cracks, through the external oxide layer and internal fuel-cladding chemical interaction layers (layer of a few microns thickness where some zirconium/ UO_2 interaction occurs), which propagated into and arrested in an oxygen stabilized alpha-Zircaloy layer. Since cracks extended only for a few microns and were arrested, their significance was small. There were no signs of either additional cladding hydriding, stress corrosion cracking (SCC), or fuel pellet degradation.

A second series of creep tests (Einziger and Kohli 1984) was performed on five PWR spent fuel rods. They were pressurized to a hoop stress of about 145 MPa, for times up to 2101 hours at 323°C. The conditions were chosen for limited annealing of in-reactor irradiation hardening. With the stresses in the range of 145 MPa, creep of 0.004% to 0.16% was observed. No cladding breaches occurred, although significant hydride agglomeration and reorientation took place in one rod that cooled under stress. Einziger and Kohli (1984) state that these high-temperature tests based on creep rupture as the limiting mechanism indicate that storage at temperatures between 400 and 440°C may be feasible for annealed rods.

Schneider and Mitchell (1992, p. 2.7), summarized experience in the foreign dry storage programs. At that time, seven countries had some fuel in dry storage. They conclude that LWR fuel can be stored for up to 100 years at temperatures of 320 to 400°C in an inert atmosphere and, if exposed to air, will last comparable times if the temperature is limited to 135 to 160°C. The Canadians have large quantities of irradiated fuel with Zircaloy cladding exposed to air with favorable results. For over eight years, they tested the effects of exposing fuel with defective cladding to moist and dry air with favorable results (no observed strain from UO_2 oxidation or cladding failure propagation).

Peehs (1998, pp.1 to 9) reviewed the performance of higher burnup fuels in dry storage casks. He reviewed the numerous possible fuel failure mechanisms and concluded that none will lead to fuel failure. His temperature profile is used for the analysis presented in Section 6.10.1.

The importance of the spent fuel dry storage experience (domestic and foreign) is that fuel failure or degradation is not expected during dry storage for the current fuels (burnups up to 50 MWd/kgU). Section 6.10.1 will analyze the potential for creep failures of very high burnup fuels with high stresses. Section 6.10.2 will analyze the potential for Delayed Hydride Cracking (DHC) for fuels with high stresses. It is also important to note that under repository conditions, most of the cladding creep or DHC failures would occur in the first 100 years after closure. This is the time when the fuel temperatures are highest and conditions closer to dry storage conditions. Dry storage is considered to be a good representation of this period.

6.10.1 Creep Failures in Dry Storage and Transportation

As noted above, no significant failures, including creep failure, have been observed to date in dry storage tests or analysis. With the potential for higher burnups in future fuels producing higher pressures and higher strains, the potential for creep failure in dry storage was evaluated. The distribution of rod stresses was developed in Section 6.7 and summarized in Figure 18. As noted before, there is a tail where 5% of the rods have hoop stresses over 62 MPa (at 27°C). These rods will have higher stresses during the time of elevated dry storage temperatures.

fail?

Best estimate dry storage temperatures were not available at the time of this analysis and the peak (center rod) temperature history for the Castor V package with 55 MWd/kgU fuel (Peehs 1998, Figure 13a) was used in this analysis. These temperatures were given for the first ten years and have been extrapolated to 20 years. In addition, a three-week period of temperatures at 350°C has been added to represent design base shipping temperatures. This temperature profile is given in Figure 24. It is conservative to use the peak design bases temperatures for all rods since most will actually see lower temperatures. Shipping will be discussed in Section 6.11 however the creep analysis is integrated so that the creep components are added. Creep failures during dry storage are combined with the creep failures during shipping because the damage is cumulative.

The creep correlation developed by Matsuo (1987, pp. 23, 26) was used and is given below.

$$\begin{aligned} E_c &= 3.62E12*(E/T)*\exp(2.4E3*\text{stress}/E)*\exp(-2.72E5/(RT)) & \text{(Eq. 6.10-1)} \\ E_s &= 1.57E13*(E/T)*[\sinh(1.13E3*\text{stress}/E)]^{2.1}*\exp(-2.72E5/RT),, \\ \text{esp} &= 2.16E-2*E_c^{0.109}, \\ \text{Strain} &= \text{esp}*(1-\exp(-52*(E_s*t)^{0.5})) + E_s*t \end{aligned}$$

where: Strain = Total Creep Strain, %

E_c , E_s , esp = Strain Components

E_c = calculated creep rate component

E_s = steady state creep rate, units = %

esp = saturated primary (transient) creep strain, units = %

Inputs:

stress = stress, MPa

t = time, hrs

T = Temperature, Kelvin

E = 114800-59.9*T, Young's modulus, MPa

R = 8.3169, gas constant, j/mole-T_k

Details of the analysis are given in Attachment III. Figure 25 gives the expected strain from both dry storage and transportation as a function of initial rod stress. Little creep occurs for rods with stresses less than 80 MPa and above that stress, the creep strain grows exponentially. Most of the creep occurs during the dry storage and only a small additional amount occurs from shipping.

To estimate what percent of the rods will fail from creep, a creep failure criteria must be established. For this, data from Chung et al. (1987, pp. 780-781) will be used. Chung et al. (1987) did a series of 20 burst tests with irradiated cladding and measured an average strain at failure of 3.3% with a range of 0.4% to 11.7%. They also did scanning electron microscope inspection of the failures and found evidence that in 11 of the tests, the failures occurred at cracks formed in the cladding from Pellet Cladding Interaction (PCI). The use of these results for a failure criteria addresses the potential for lower failure strains from pre-existing internal cracks and that failure might not be a pure material creep.

There is corroborating evidence for using this failure criteria. In the German (Peehs) model (Pescatore et al. 1990, p. 39), a conservative value for a strain at which cladding failure occurs, 1% strain, was selected. Sanders et al. (1992, p. III-53) recommends a median value of 6 percent for rupture strain and also reports a series of experiments with irradiated cladding that had a median failure strain of 4% Sanders et al. (1992, p. III-51). Van Swam et al. (1997b, p. 430) report 8 ring tensile tests on irradiated cladding with the resulting total elongation being 7.6% (1.5% to 15% range) at room temperature and 15.8% (5% to 21% range) at 350°C. These results suggest that the creep failure criteria being used are very conservative because of the effect of the elevated temperatures. The Technical Basis Document (CRWMS M&O 1998b, Table 6-19, p.6-14), showed 54 tensile tests or high temperature rod creep tests. The average uniform elongation strain for these tests is 4%. A failure criteria of 3.3% is used in this analysis to predict creep failure and is more conservative (lower) than most other reported values, especially since no correction has been made for the elevated temperatures.

Using a strain limit of 3.3% (range 0.4% to 11.7%) in Figure 25, an initial room temperature stress of 112 MPa is required for the rod to fail from creep. The CCDF for initial rod stress was presented in Figure 18 and has been redrawn as Figure 26 using a logarithmic scale to better define the tail of the distribution. About 0.24% (with range 0 to 4.4% of the rods are expected to fail in dry storage and transportation from creep. Transportation contributed about 0.01% of that total 0.24%.

The strain depends strongly on the temperature (an Arrhenius relationship in Equation 6.10-1) and this analysis was performed using peak cladding temperatures. If actual dry storage and shipping temperatures were available and stayed below 300°C, the failure rate would have been closer to zero. This demonstrates the degree of conservatism made in using peak temperatures.

6.10.2 DHC Failures in Dry Storage

During Delayed Hydride Cracking (DHC), hydrides slowly form at a crack tip until the crack propagates through the hydride region at the crack tip and the crack propagation stops. This sequence repeats itself and the crack propagates slowly through the metal. The hydrides preferentially collect at the crack tip because the tensile stress reduced the solubility of the hydride in that region. The critical stress intensity factor (K_{IH}) is the minimum stress intensity that will permit any DHC, regardless of velocity (velocity approaches 0). For this analysis, the stress intensities (K_I) will be calculated and compared to the K_{IH} . If $K_I > K_{IH}$, then the crack will start to propagate and, it is assumed, because of long repository times, failure will occur. DHC failure occurred in some zirconium coolant tubes in a Candu reactor where high temperature gradients caused excess hydride buildup in a specific location.

The stress intensity factor, K_I , is a measure of the increased stress at the tip of a crack. The stress intensity factor is proportional to the far-field stress times the square root of the crack length. For a sharp crack, a limiting case, the stress intensity factor is the Reed-Hill (1973, p. 800) equation, substituting w (the crack depth) for c (the crack length), where the relationship is the crack depth = $\frac{1}{2}$ crack length from Dieter (1976, p. 191):

$$K_I = St * (\pi * w)^{0.5}$$

(Eq. 6.10-2)

check stress in IRSK
- localization of corrosion

where: K_I = stress intensity factor, $\text{MPa}\cdot\text{m}^{0.5}$

St = cladding stress, MPa

w = crack depth, m

The calculated crack size distribution is discussed in Section 6.6 and given in Figure 17. The median ($P = 50$ percent) value is $12.6 \mu\text{m}$, median was $19 \mu\text{m}$ and the largest size crack in the 2000 samplings was $119 \mu\text{m}$. The calculated stress distribution is given in Figures 18 and 26. DHC is unlikely at temperatures above 260°C (Mahmood et al. 1998 p.20), because of the plasticity of the material. Rothman (1984, p. 37) reports that DHC is unlikely above 250°C because of plasticity of the material. For this calculation, the temperature of 260°C is assumed and the pressure is adjusted accordingly. The crack size distribution and stress distribution can be combined to give a distribution of stress intensity factors, K_I , given in Figure 27. Some of the properties of this distribution of the stress intensity factor are:

Mean: $0.44 \text{ MPa}\cdot\text{m}^{0.5}$

Median: $0.40 \text{ MPa}\cdot\text{m}^{0.5}$

95%: $0.097 \text{ MPa}\cdot\text{m}^{0.5}$

5%: $1.078 \text{ MPa}\cdot\text{m}^{0.5}$

maximum: $2.7 \text{ MPa}\cdot\text{m}^{0.5}$

minimum: $1.61\text{E-}03 \text{ MPa}\cdot\text{m}^{0.5}$

The threshold stress intensity factor (K_{IH}) is the minimum stress intensity where crack propagation is expected. The work of Shi and Puls (1994, p. 239, Fig. 7), shows experimental K_{IH} in the range of 5 to $12 \text{ MPa}\cdot\text{m}^{0.5}$ for Zr-2.5% Nb. Rothman (1984, p. 37), reports uses a K_{IH} of $6 \text{ MPa}\cdot\text{m}^{0.5}$ for Zircaloy-2. Pescatore et al. (1990, table 6, p.50) report values of 10 and 14. Huang (1995, p. 188) shows K_{IH} for irradiated Zircaloy-2 approaching $6 \text{ MPa}\cdot\text{m}^{0.5}$. For this work, Huang's and Rothman's value for irradiated cladding of $6 \text{ MPa}\cdot\text{m}^{0.5}$ was used. Because the observed values of K_I are well below these values, exactly which value of K_{IH} selected is not important. No values in our sampling of rods have K_I s neat the threshold stress intensity value. The maximum observed K_I was $2.7 \text{ MPa}\cdot\text{m}^{0.5}$ and the mean value was $0.44 \text{ MPa}\cdot\text{m}^{0.5}$.

5% of
crack
& Top

Rothman (1984, pp. 33 - 39) reviewed DHC in Zircaloy cladding in a repository. Rothman concludes that DHC is unlikely unless the fuel rods have large existing cracks (50 percent of wall thickness) and very high stresses (137 MPa). He also concludes that hydride reorientation is also unlikely because of the lack of large temperature gradients in the repository and the cladding stresses are lower than needed for reorientation. Peehs (1998, pp. 5, 6) concluded that neither DHC nor hydride reorientation would occur in dry storage.

In conclusion, failure of the cladding by DHC in dry storage is unlikely and has not been included in the abstraction for the GOLDSIM computer code analysis. Stresses (and stress intensity factors) are too low for crack propagation.

6.11 ROD FAILURE DURING FUEL SHIPMENT

During normal shipping of fuel, no failures have been identified in the literature. Sanders et al. (1992) analyzed transportation accidents. Failure probabilities were calculated for a specific drop test height of nine meters (9m), a 0.3-m drop, and normal transport, (i.e., normal vibration). The 9-m drop was by far the most severe, with failure probabilities of the order of 10^{-4} , compared to 10^{-8} to 10^{-12} for the other events. This reference generated acceleration versus frequency curves for truck and rail shipping. It then looked at structural damage from a union of the hazard curves and the structural model and concluded that no additional damage is done in shipping.

In "Dynamic Impact Effects on Spent Fuel Assemblies," Witte et al. (1989) performed an analytical evaluation of the potential impacts of all movements. They conclude (Witte et al. 1989, p. 5) that no yielding of the rods would occur below 63g's acceleration. Normal transport would result in accelerations below these values.

IAEA (1988, p. 114) surveyed shipping worldwide and reported that "to date, there have been no major incidents during 30 years experience connected with irradiated fuel transport."

Table 11 (CRWMS M&O 1999) summarizes the design base maximum cladding temperatures reported by numerous vendors in their SARs. The SAR docket numbers ~~is~~^{are} also included in this table. The design base temperatures are upper limit ones and most if not all of the actual fuel should be below this temperature. The range of temperatures is 242°C to 378°C with a mean peak temperature of 322°C. Creep failures during shipment are combined with the creep failures during dry storage because the damage is cumulative. This analysis is discussed in Section 6.10.1 and the analysis is presented in Attachment III. For the creep analysis performed in Section 6.10.1 that considered dry storage and shipping, a peak cladding temperature for transportation of 350°C was used. This temperature is 28°C above the mean value. It is consistent with the initial dry storage temperature and the cladding temperature limit currently used at YMP. It was also assumed that the shipment took three weeks and the temperature was at the peak value for that interval. As noted in Section 6.10.1, shipping added 0.01% of the total rod failure of 0.24%. As noted in Section 6.10.2, no Delayed Hydride Cracking (DHC) is expected at the maximum DHC temperature of 260°C, including during transportation.

pre down
+
backfill

Table 11. Comparison of Maximum Cladding Design Temperatures for Shipping Casks (CRWMS M&O, 1999)

| Vendor | Type | Canister | Max. Cladding Temp. | Source |
|----------------------------|--------------|---------------------|---|--|
| NAC | STC | Yes | 302C Rev 10 is latest rev listing cladding temp. | NAC-STC SAR, Docket 71-235 Rev. 10, 2/99 (Note: Latest version is Rev. 12, 4/30/99) |
| NAC | STC | No | 309C Rev 10 is latest rev listing cladding temp. | NAC-STC SAR, Docket 71-235 Rev. 10, 2/99 (Note: Latest version is Rev. 12, 4/30/99) |
| Holtec International, Inc. | HI-STAR 100 | Yes MPC-68 (BWR) | 378C | Hi-STAR SAR Docket 71-9261, Report HI-951251, Rev. 8 |
| Holtec International, Inc. | HI-STAR 100 | Yes MPC-24 (PWR) | 372C | Hi-STAR SAR Docket 71-9261, Report HI-951251, Rev. 8 |
| Westinghouse | WESFLEX W21 | Yes | 321C | WESFLEX W21 SAR, Docket 71-9276, Rev. 0, 6/19/98 |
| Westinghouse | WESFLEX W44 | Yes | 321C | WESFLEX W44 SAR, Docket 71-9276, Rev. 0, 6/12/98 |
| Westinghouse | WESFLEX W74 | Yes | 330C | WESFLEX W74 SAR, Docket 71-9276, Rev. 0, 5/29/98 |
| Transnuclear West | NUHOMS MP187 | Yes | 669F/354C Rev 3 is latest rev listing cladding temp. | SAR for NUHOMS-MP187 Multi-Purpose Cask, Docket 71-09255, Rev 3, 7/31/97 (Note: Latest version is Rev. 7) |
| Transnuclear | TN-68 | | 490F/254C @ -20F ambient; 388F/198C @ -40F ambient | TN-68 Transport Packaging SAR, Docket 71-09293, Rev 0, 4/30/99 |
| Chem Nuclear | IF-300 | | 685F/363C per Table A-3.4-3 | Application for Renewal of COC 9001 for Vectra IF-300 Shipping Cask, Docket 71-09001, Rev 3/30/95 |
| GNB | GNS-16 | | 242C per Table 10 | Application Documents for Trans. Licensing GNS 16 SAR, Rev 1, 5/28/98 |

The importance of the fuel transportation analysis and experience (domestic and foreign) is in demonstrating that very little fuel failure or degradation is expected during transportation. The use of actual temperatures instead on design temperatures would reduce the small fraction of fuel damaged during transportation.

7. CONCLUSIONS

The purpose of this analysis is to describe the condition of the commercial nuclear fuel as it is received at the YMP site. This analysis generates the initial boundary condition for the analysis of degradation of the fuel in the repository. Table 12 summarizes the distributions of the various properties developed in this analysis. These distributions are given in the Excel file: Rod-Initial-C.xls and accessible through data tracking number DTN TBD. The CCDFs for the various parameters are not independent. They are generated using a single burnup distribution and must be used accordingly. Creep failures in the repository must be coupled with the creep failures in dry storage since rods predisposed to fail during the repository thermal cycle have already received some creep (and possible failure) during dry storage.

Table 12. CCDFs Describing Expected Fuel Stream into YMP

| Property | Report Section | Mean Value | Upper 5% Value | CCDF Figure |
|--------------------------------|----------------|---------------------------|---------------------------|-------------|
| Burnup | 6.2 | 44.1 MWd/kgU | 63.3 MWd/kgU | 3 |
| Internal Pressure | 6.3.6 | 4.8 MPa | 7.3 MPa | 9 |
| Oxide Thickness | 6.4 | 52 μm | 112 μm | 13 |
| Hydride Content | 6.5 | 358 ppm | 738 ppm | 15 |
| Crack Size | 6.6 | 12.6 μm | 57 μm | 17 |
| Stress | 6.7 | 38.4 MPa | 61.8 MPa | 18, 26 |
| Stress Intensity Factor, K_I | 6.10.2 | 0.44 MPa-m ^{0.5} | 1.08 MPa-m ^{0.5} | 27 |

Table 13 gives the percent of rods that have failed cladding at emplacement. Failures from fuel handling are included in the reactor failures and dry storage failures. These fuel rods will be available for cladding unzipping and fuel dissolution when the WP fails. Additional rods will fail and also be available for dissolution from degradation in the repository, depending on the repository and WP conditions. The analysis of rod degradation in the repository is addressed in other AMRs.

Table 13. Percent and Cause of Rods failed in a WP

| Rod Failure Mode | Percent of Rods Failed/WP |
|---|---------------------------|
| Reactor Operation incl. Incipient Failures (Mean) | 0.109 Range: 0.0 to 5.2 |
| Pool Storage | 0.0 |
| Dry Storage | 0.045 |
| Dry Storage & Transportation, Creep | 0.24 |
| Dry Storage & Transportation, DHC | 0.0 |
| Transportation (Vibration, Impact) | 0.01 |
| Fuel Handling | (Included in above) |
| Total | 0.404 Range: 0.30 to 5.5 |

The shape of the distribution function for the percent of rods failed in a WP is based on the assumption that the WPs are loaded with fuel in the order of reactor discharge. This assumption means that fuel from periods with very poor performance is placed in the same WP and increases the range of distribution. The periods of poor performance were in the 1970s. These fuels have lower burnups and are cooler than the newer fuels and would probably be blended with newer, hotter fuels to meet thermal loading goals. Assuming that no blending occurs, the CCDF for

failed cladding in a WP is given in Table 14. This CCDF is the sum of the reactor failure CCDF given in Figure 21 and the other failures listed in Table 13. For square arrays in reactors, the uncertainty for failures of adjacent fuel rods is a factor of 4 because the fuel is square and each rod has 4 adjacent rods. The failures included in Table 14 are shipping, dry storage, breaches during reactor operation, but excluding creep and cumulative damage.

Table 14. CCDF for Rods with Failed Cladding in a WP

| CCDF PWR & BWR | Lower Unc. | % failure Incl. All | Upper Unc |
|-------------------|------------|------------------------|-----------|
| 1.000 | 0.014 | 0.055 | 0.220 |
| 0.999 | 0.015 | 0.058 | 0.234 |
| 0.983 | 0.016 | 0.062 | 0.249 |
| 0.856 | 0.018 | 0.072 | 0.287 |
| 0.653 | 0.021 | 0.085 | 0.340 |
| 0.582 | 0.022 | 0.090 | 0.358 |
| 0.506 | 0.024 | 0.095 | 0.379 |
| 0.260 | 0.028 | 0.114 | 0.454 |
| 0.198 | 0.036 | 0.145 | 0.578 |
| 0.110 | 0.050 | 0.202 | 0.807 |
| 0.098 | 0.052 | 0.209 | 0.836 |
| 0.077 | 0.074 | 0.296 | 1.186 |
| 0.065 | 0.075 | 0.298 | 1.193 |
| 0.051 | 0.080 | 0.321 | 1.285 |
| 0.038 | 0.125 | 0.499 | 1.996 |
| 0.033 | 0.247 | 0.987 | 3.950 |
| 0.022 | 0.289 | 1.157 | 4.627 |
| 0.020 | 0.450 | 1.799 | 7.194 |
| 0.019 | 0.509 | 2.035 | 8.141 |
| 0.012 | 0.694 | 2.776 | 11.103 |
| 0.004 | 0.763 | 3.051 | 12.202 |
| 0.0002 | 1.321 | 5.286 | 21.142 |
| 0.000 | 1.321 | 5.286 | 21.142 |

8. REFERENCES

Andrews, M.G. and Matzie, R.A. 1985. "A Report on the Reliability, Performance and Progress of Combustion Engineering's Fuel Assemblies toward Extended Burnup." *Proceedings of the American Nuclear Society Topical Meeting on Light Water Reactor Fuel Performance, Orlando, Florida, April 21-24, 1985, 1*, 2-42. La Grange, Illinois: American Nuclear Society, Inc. TIC: 226810.

Bailey, W. E.; Marlowe, M. O.; and Proebstle, R. A. 1985. "Trends in BWR Fuel Performance." *Proceedings of the American Nuclear Society Topical Meeting on Light Water Reactor Fuel Performance, Orlando, Florida, April 21-24, 1985, 1*, 1-3. La Grange Park, Illinois: American Nuclear Society, Inc. TIC: 226810.

Bailey, W. J. and Wu, S. 1990. *Fuel Performance Annual Report for 1988*. NUREG/CR-3950. Richland, Washington: Pacific Northwest Laboratory. TIC: 245644.

Bain, G. M.; McInteer, W. A.; Papazoglou, T. P. 1985. "Release and Migration of Fission Products in High Burnup Fuel." *Proceedings of the American Nuclear Society Topical Meeting on Light Water Reactor Fuel Performance, Orlando, Florida, April 21-24, 1985, 2*, 4-1 & 4-13. La Grange Park, Illinois: American Nuclear Society, Inc. TIC: 226810.

Barner, J. O. 1985. *Characterization of LWR Spent Fuel MCC-Approved Testing Material - ATM 101*. PNL-5109, Rev. 1. Richland, Washington: Pacific Northwest Laboratory. TIC: 216710.

Berggren, G 1980. "Helium Retention - Summary of Reports and Memoranda." *Studsvik Energiteknik AB 1980-02-14.*, 4. Stockholm, Sweden: . Svensk Karnbransleforsorjning AB Project Karnbranslesakerhet. TIC: 205784.

Charquet, D.; Rudling, P.; Mikes-Lindback, M.; and Barberis, P. 1994. "Hydrogen Absorption Kinetics During Zircaloy Oxidation in Steam." *Zirconium in the Nuclear Industry, Tenth International Symposium, Baltimore, Maryland, June 21-24, 1993*, 80-95. Philadelphia, Pennsylvania: American Society for Testing and Materials. TIC: 237257.

Chung, H. M.; Yaggee, F. L.; and Kassner, T. F. 1987. "Fracture Behavior and Microstructural Characteristics of Irradiated Zircaloy Cladding." *Special Technical Publication, 0 (939)*, 775. Philadelphia, Pennsylvania: American Society for Testing and Materials. TIC: 238255

CRWMS M&O 1998a. *Design Basis Cladding Analysis*. BBA000000-01717-0200-00054 REV 01. Las Vegas, Nevada: CRWMS M&O. ACC: MOL.19980325.0102.

CRWMS M&O 1998b. *Waste Form Degradation, Radionuclide Mobilization, and Transport through the Engineered Barrier System.* Chapter 6 of *Total System Performance Assessment - Viability Assessment (TSPA-VA) Analyses Technical Basis Document*. B00000000-01717-4301-00006 REV 01. Las Vegas, Nevada: CRWMS M&O. ACC: MOL.19981008.0006.

CRWMS M&O 1999. Eble, R.G. 1999. MGR Transportation Temperatures Preliminary Information Memorandum to Eric Siegmann, August 31, 1999. MOL.19991105.0079.

Dieter, G.E. 1976. *Mechanical Metallurgy*. 2nd Edition. New York, New York: McGraw-Hill Book Company. On Order

Dehon, C.; Cambon, J. L.; Houdaille, B.; and Chagrot, M 1985. "Main Results from Fragma Fuel Performance in Power Reactors." *Proceedings of the American Nuclear Society Topical Meeting on Light Water Reactor Fuel Performance, Orlando, Florida, April 21-24, 1985, 1, 2-24*. La Grange Park, Illinois: American Nuclear Society. TIC: 226810.

DOE (U.S. Department of Energy) 1992. *Characteristics of Potential Repository Wastes*. DOE/RW-0184-R1. Volume 1. Washington, D.C.: U.S. Department of Energy, Office of Civilian Radioactive Waste Management. ACC: HQO.19920827.0001.

DOE (U.S. Department of Energy) 1996. *Spent Nuclear Fuel Discharges from U.S. Reactors 1994*. SR/CNEAF/96-01. Washington, D.C.: U.S. Department of Energy, Energy Information Administration. TIC: 232923.

Duke Energy. 1997. *McGuire Nuclear Station PRA Revision 2 Summary Report*. Duke Power, Charlotte, NC, December 1997 TIC: (submitted).

Einzigler, R.E. and Kohli, R. 1984. "Low-Temperature Rupture Behavior of Zircaloy-Clad Pressurized Water Reactor Spent Fuel Rods Under Dry Storage Conditions." *Nuclear Technology*, 67 (1), 107-123. Hinsdale, Illinois: American Nuclear Society. TIC: 216868.

Einzigler, R.E.; Atkin, S.D.; Stellrecht, D.E.; and Pasupathi, V. 1982. "High Temperature Postirradiation Materials Performance of Spent Pressurized Water Reactor Fuel Rods Under Dry Storage Conditions." *Nuclear Technology*, 57 (1), 65-80. Hinsdale, Illinois: American Nuclear Society. TIC: 237142.

EPRI (Electric Power Research Institute) 1997. *The Technical Basis for the Classification of Failed Fuel in the Back-End of the Fuel Cycle*. EPRI TR-108237. Palo Alto, California: Electric Power Research Institute. TIC: 236839

Essig, T.H. 1999. Acceptance for Referencing of Framatome Cogema Fuels Topical Report BAW-10186P: "Extended Burnup Evaluation" (TAC NO MA3705) Letter Report ACC: MOL.19990927.0213.

Garde, A.M. 1986. *Hot Cell Examination of Extended Burnup Fuel from Fort Calhoun*. DOE/ET/34030-11. Windsor, Connecticut: Combustion Engineering. TIC: 237128.

Garde, A.M. 1991. "Enhancement of Aqueous Corrosion of Zircaloy-4 Due to Hydride Precipitation at the Metal-Oxide Interface." *Zirconium in the Nuclear Industry, Ninth International Symposium, Kobe, Japan, November 5-8, 1990*. ASTM Special Technical

Publication, 1, 566 - 599. Philadelphia, Pennsylvania: American Society for Testing and Materials. TIC: 237129.

Guenther, R. J.; Blahnik, D. E.; Campbell, T. K.; Jenquin, U. P.; Mendel, J. 1988a. *Characterization of Spent Fuel Approved Testing Material -ATM-103.* PNL-5109-103. Richland, Washington: Pacific Northwest Laboratory. TIC: 223979.

Guenther, R. J.; Blahnik, D. E.; Campbell, T. K.; Jenquin, U. P.; Mendel, J. 1988b. *Characterization of Spent Fuel Approved Testing Material -ATM-106.* PNL-5109-106. Richland, Washington: Pacific Northwest Laboratory. TIC: 223978.

Guenther, R. J.; Blahnik, D. E.; Jenquin, U. P.; Mendel, J. E.; Thomas, L. E.; a 1991. . *Characterization of Spent Fuel Approved Testing Material -ATM-104.* PNL-5109-104. Richland, Washington: Pacific Northwest Laboratory. TIC: 203846.

Huang, F.H. 1995. *Fracture Properties of Irradiated Alloys.* 195. Richland, Washington: Avante Press. TIC: 224548.

IAEA (International Atomic Energy Agency) 1988. *Survey of Experience with Dry Storage of Spent Nuclear Fuel and Update of Wet Storage Experience.* IAEA-TECDOC-290. 178. Vienna, Austria: International Atomic Energy Agency. TIC: 233246

Johnson, A.B., JR 1977. *Behavior of Spent Nuclear Fuel in Water Pool Storage.* BNWL-2256. Richland, Washington: Pacific Northwest Laboratory. TIC: 234703.

Johnson, A.B., Jr.; Bailey, W.J.; Schreiber, R.E.; and Kustas, F.M. 1980. *Annual Report - FY 1979. Spent Fuel and Fuel Pool Component Integrity.* PNL-3171. Richland, Washington: Pacific Northwest Laboratory. TIC: 229623.

Johnson, A.B., Jr.; Dobbins, J.C.; Zaloudek, F.R.; Gilbert, E.R.; and Levy, I.S. 1987. *Assessment of the Integrity of Spent Fuel Assemblies Used in Dry Storage Demonstrations at the Nevada Test Site.* PNL-6207. Richland, Washington: Pacific Northwest Laboratory. TIC: 230135

Lanning, D.D.; Beyer, C.E.; and Painter, C.L. 1997. *FRAPCON-3: Modifications to Fuel Rod Material Properties and Performance Models for High-Burnup Application.* NUREG/CR-6534-Volume 1. Richland, Washington: Pacific Northwest Laboratory. TIC: 238923.

Lide, D. R. and Frederikse, H. P. R. 1997. *CRC Handbook of Chemistry and Physics.* 78th Edition, CRC Press, Boca Raton. TIC: 243741.

Mahmood, S.T.; Farkas, D.M.; Adamson, R.B.; and Etoh, Y. 1998. "Post-Irradiation Characterization of Ultra High Fluence Zircaloy-2 Plate." *Twelfth International Symposium on Zirconium in the Nuclear Industry, Program Abstracts, Toronto, Ontario, Canada, June 15-18,*

1998, 19-20. Philadelphia, Pennsylvania: American Society for Testing and Materials. TIC: 237270.

Manaktala, H.K. 1993. *Characteristics of Spent Nuclear Fuel and Cladding Relevant to High-Level Waste Source Term*. CNWRA 93-006. San Antonio, Texas: Center for Nuclear Waste Regulatory Analyses. TIC: 208034.

Manzel, R. and Coquerelle, M. 1997. "Fission Gas Release and Pellet Structure at Extended Burnup." *Proceedings of the 1997 International Topical Meeting on LWR Fuel Performance, Portland, Oregon, March 2-6, 1997*, 463-470. La Grange Park, Illinois: American Nuclear Society. TIC: 232556.

Mardon, J.P.; Garner, G.; Beslu, P.; Charquet, D.; and Senevat, J. 1997. "Update on the Development of Advanced Zirconium Alloys for PWR Fuel Rod Claddings." *Proceedings of the 1997 International Topical Meeting on Light Water Reactor Fuel Performance, Portland, Oregon, March 2-6*, 405-412. La Grange Park, Illinois: American Nuclear Society, Inc. TIC: 243519.

Matsuo, Y. 1987. "Thermal Creep of Zircaloy-4 Cladding Under Internal Pressure." *Journal of Nuclear Science and Technology*, 24 (2), 111-119. Tokyo, Japan: Atomic Energy Society of Japan. TIC: 237137.

McDonald, S.G. and Kaiser, R.S. 1985. "The Impact of Metallic Debris on Fuel Performance - A Case History." *Proceedings of American Nuclear Society Topical Meeting on Light Water Reactor Fuel Performance, Portland, Oregon, April 29-May 3, 1979*, 2/3 to 2/19. La Grange Park, Illinois: American Nuclear Society, Inc. TIC: 243519.

McKinnon, M.A. and Doherty, A.L. 1997. *Spent Nuclear Fuel Integrity During Dry Storage - Performance Tests and Demonstrations*. PNNL-11576. Richland, Washington: Pacific Northwest Laboratory. TIC: 237126.

Morel, M.; Melin, P.; and Dumont, A. 1994. "Updated Status of In Reactor Experience of Framema Fuel Products." *Proceedings of the 1994 International Topical Meeting on Light Water Reactor Fuel Performance, West Palm Beach, Florida, April 17-21, 1994*, 15-21. La Grange Park, Illinois: American Nuclear Society. TIC: 243043.

Pati, S. R. and Garde, A. M. 1985. "Fission Gas Release from PWR Fuel Rods at Extended Burnups." *Proceedings of the American Nuclear Society Topical Meeting on Light Water Reactor Fuel Performance, 2*, 4-28. La Grange Park, Illinois: American Nuclear Society, Inc. TIC: 226810.

Peehs, M. 1998. *Assessment of Dry Storage Performance of Spent LWR Fuel Assemblies with Increasing Burn-Up*. Erlangen, Germany: Siemens KWU-NBT. TIC: 245171.

Pescatore, C.; Cowgill, M.G.; and Sullivan, T.M. 1989. *Zircaloy Cladding Performance under Spent Fuel Disposal Conditions Progress Report May 1 - October 31, 1989*. BNL 52235. Upton, New York: Brookhaven National Laboratory. ACC: NNA.19900710.0055.

Potts, G.A. and Proebstle, R.A. 1994. "Recent GE BWR Fuel Experience." *Proceedings of the 1994 International Topical Meeting on Light Water Reactor Fuel Performance, West Palm Beach, Florida, April 17-21, 1994*, 87-95. La Grange Park, Illinois: American Nuclear Society. TIC: 243043.

Preble, E. A.; Painter, C. L.; Alvis, J. A.; Berting, F. M.; Beyer, C. E.; Payne 1993. *Fuel Performance Annual Report for 1990*. NUREG/CR-3950, Volumn 8. Richland, Washington: Pacific Northwest Laboratory. TIC: 245486.

Ravier, G.; Masuy, G.; and Willse, J. T. 1997. "Framatome and FCF Recent Operating Experience and Advanced Features to Increase Performance and Reliability." *Proceedings of the American Nuclear Society 1997 International Topical Meeting on Light Water Reactor Fuel Performance, Portland, Oregon, March 2-6, 1997*, 34. La Grange Park, Illinois: American Nuclear Society, Inc. TIC: 243519.

Reed-Hill, R.E. 1973. *Fuel in a Tuff Repository* in *Physical Metallurgy Principles*. Second Edition. 797-801. New York, New York: D. Van Nostrand Company. TIC: 237154.

Roark, R.J.. 1989. *Roark's Formulas for Stress and Strain*. 6th Edition. New York, New York: McGraw-Hill. TIC: 10191.

Rothman, A.J. 1984. *Potential Corrosion and Degradation Mechanisms of Zircaloy Cladding on Spent Nuclear Fuel in a Tuff Repository*. UCID-20172. Livermore, California: Lawrence Livermore National Laboratory. ACC: NNA.19870903.0039.

Sanders, T.L.; Seager, K.D.; Rashid, Y.R.; Barrett, P.R.; Malinauskas, A.P.; Einziger, R.E.; Jordan, H.; Duffey, T.A.; Sutherland, S.H.; and Reardon, P.C. 1992. *A Method for Determining the Spent-Fuel Contribution to Transport Cask Containment Requirements*. SAND90-2406. Albuquerque, New Mexico: Sandia National Laboratories. TIC: 232162.

Sasaki, S. and Kuwabara, S. 1997. "Utility Perspective on Commercial Light-Water Reactor Fuel in Japan." *Proceedings of the 1997 International Topical Meeting on Light Water Reactor Fuel Performance, Portland, Oregon, March 2-6, 1997*, 11-20. La Grange Park, Illinois: American Nuclear Society. TIC: 237169.

Sayles, C.W.; Chang, R.Y.; Thomsen, O.J.; and Swoope, S.C. 1994. "4. Use of Axial Cesium Distribution for Failure Identification in San Onofre Units." *Transactions of the American Nuclear Society, New Orleans, Louisiana, June 19-23, 1994*, 70, 76-77. La Grange Park, Illinois: American Nuclear Society. TIC: 236801.

Schneider, K.J. and Mitchell, S.J. 1992. *Foreign Experience on Effects of Extended Dry Storage on the Integrity of Spent Nuclear Fuel*. PNL-8072. Richland, Washington: Pacific Northwest Laboratory. TIC: 205836.

Schrire, D.I. and Pearce, J.H. 1994. "Scanning Electron Microscope Techniques for Studying Zircaloy Corrosion and Hydriding." *Zirconium in the Nuclear Industry, Tenth International Symposium, Baltimore, Maryland, June 21-24, 1993*. ASTM Special Technical Publication 1245. Garde, A.M. and Bradley, E.R., eds, 98-115. Philadelphia, Pennsylvania: American Society for Testing and Materials. TIC: 237130.

Shi, S.Q. and Puls, M.P. 1994. "Criteria for Fracture Initiation at Hydrides in Zirconium Alloys I. Sharp Crack Tip." *Journal of Nuclear Materials*, 208 (3), 232-242. Amsterdam, The Netherlands: North-Holland Publishing Company. TIC: 237135.

Smith, G.P., Jr.; Pirek, R.C.; Freeburn, H.R.; and Schrire, D. 1994. *The Evaluation and Demonstration of Methods for Improved Nuclear Fuel Utilization*. DOE/ET/34013-15. Washington, D.C.: U.S. Department of Energy. TIC: 245407.

Sunderland, D.J.; Kennard, M.W.; and Harbottle, J.E. 1994. "2. Identification of Failed LWR Fuel in U.S. Reactors." *Transactions of the American Nuclear Society*, 70, 73-74. La Grange Park, Illinois: American Nuclear Society. TIC: 237153.

VanSwam, L.F.; Bain, G. M.; Dey, W. C.; Davis, D. D.; and Heckermann, H. 1997a. "BWR and PWR fuel Performance at High Burnup." *Proceedings of the 1997 International Topical Meeting on LWR Fuel Performance, Portland, Oregon, March 2-6, 1997*, 455-460. La Grange Park, Illinois: American Nuclear Society. TIC: 232556.

Van Swam, L.F.; Strasser, A.A.; Cook, J.D.; and Burger, J.M. 1997b. "Behavior of Zircaloy-4 and Zirconium Liner Zircaloy-4 Cladding at High Burnup." *Proceedings of the 1997 International Topical Meeting on LWR Fuel Performance, Portland, Oregon, March 2-6, 1997*, 421-431. La Grange Park, Illinois: American Nuclear Society. TIC: 232556.

Wilson, H.W.; Menke, H.F.; Kunishi, H; Miller, R.S.; and Scherpereel, L.R. 1997. "Westinghouse Fuel Performance in Today's Aggressive Plant Operating Environment." *Proceedings of the 1997 International Topical Meeting on LWR Fuel Performance, Portland Oregon, March 2-6, 1997*, 23-30. La Grange Park, Illinois: American Nuclear Society. TIC: 243519.

Witte, M.C.; Chun, R.C.; and Schwartz, M.W. 1989. "Dynamic Impact Effects on Spent Fuel Assemblies." *9th International Symposium on the Packaging and Transportation of Radioactive Materials Proceedings, Washington, D.C., June 11-16, 1989*, 1, 186-194. Oak Ridge, Tennessee: Oak Ridge National Laboratory. TIC: 240741.

Yang, R.L. 1997. "Meeting the Challenge of Managing Nuclear Fuel in a Competitive Environment." *Proceedings of the 1997 International Topical Meeting on LWR Fuel Performance, Portland, Oregon, March 2-6, 1997*, 3-10. La Grange Park, Illinois: American Nuclear Society. TIC: 232556.

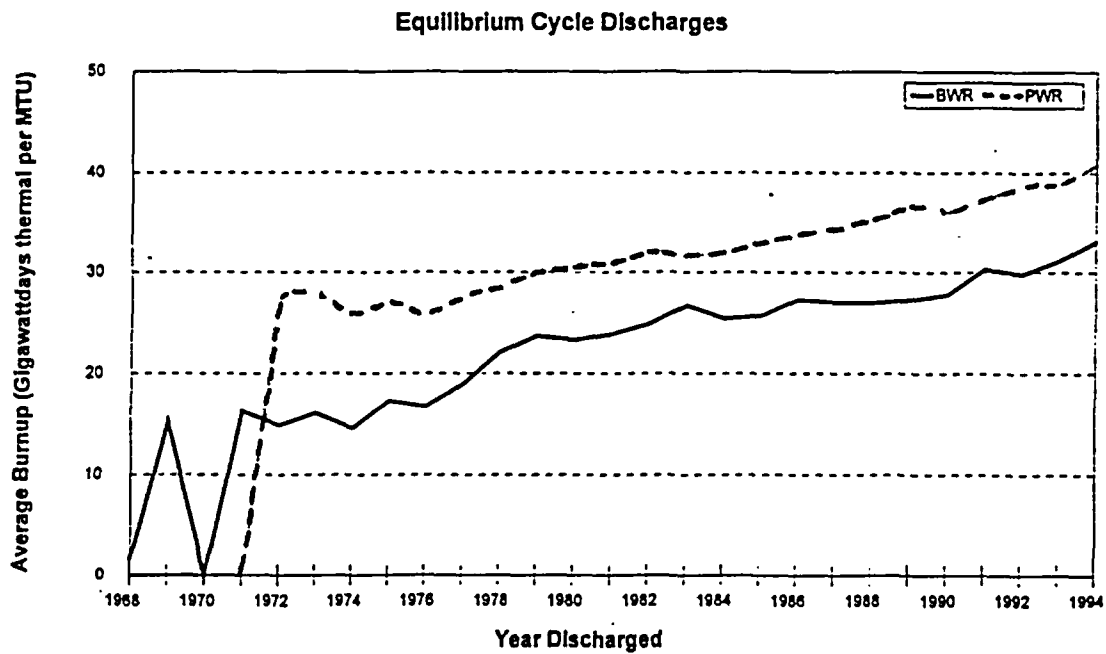


Figure 1. Equilibrium Cycle Discharge vs. Calendar Year (from DOE 1996)

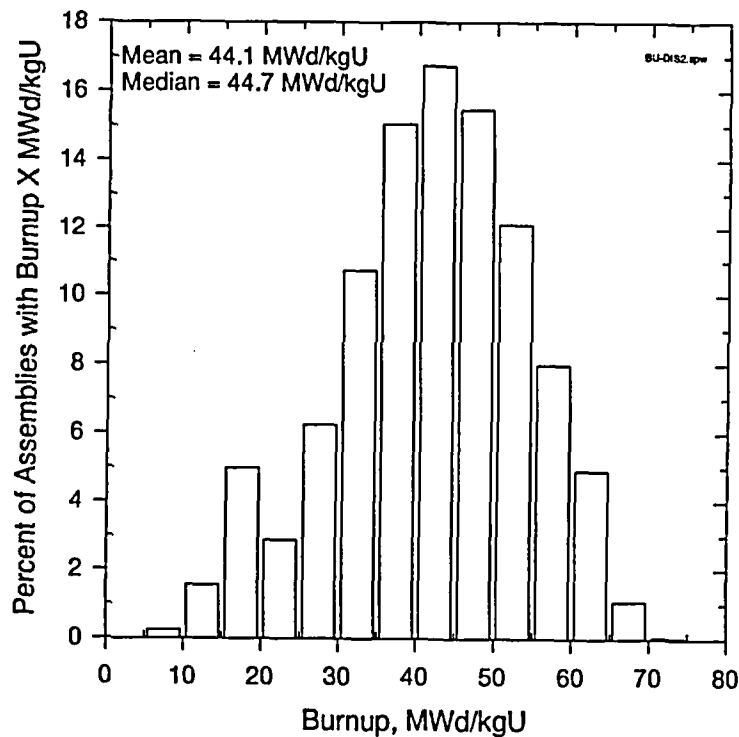


Figure 2. Expected Burnup Distribution for PWR Assemblies

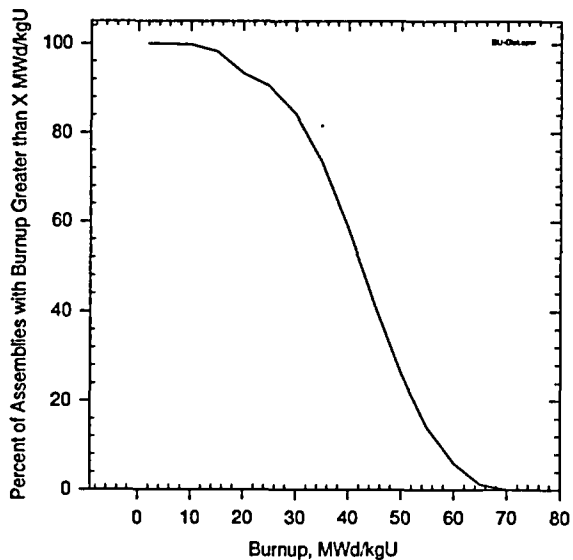


Figure 3. Distribution of Assembly Burnup

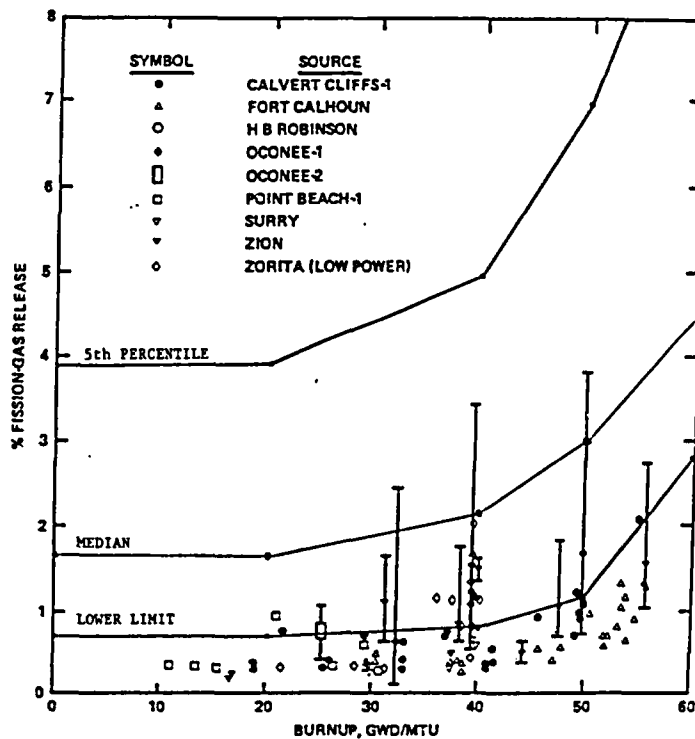


Figure 4. Fission Gas Release for U.S. PWR fuel Rods (from Garde 1986)

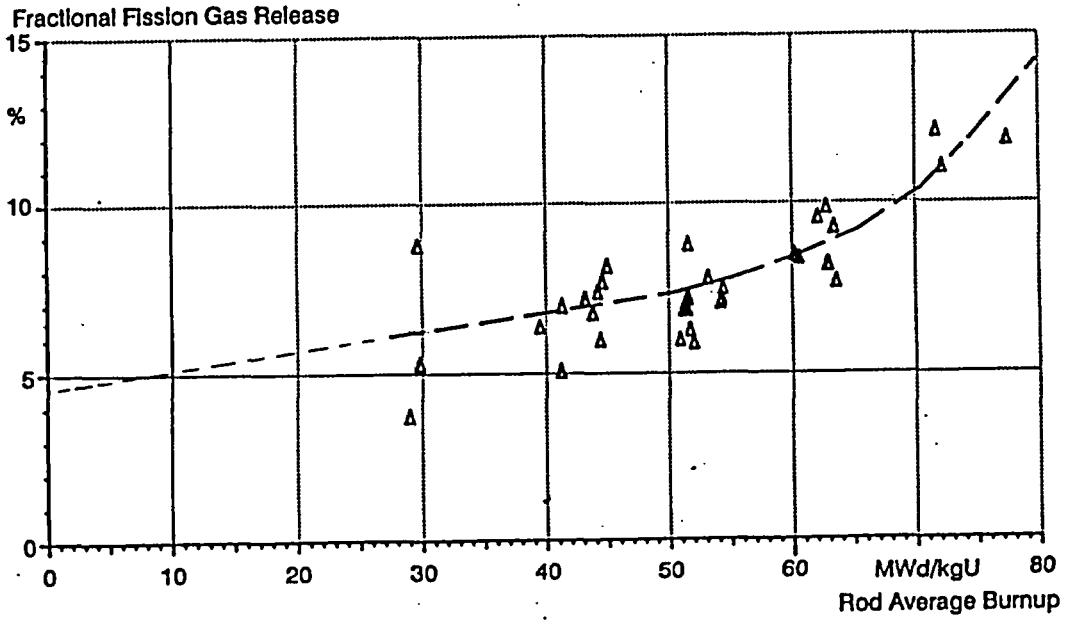


Figure 5. Fission Gas Release vs. Burnup (from Manzel and Coquerelle 1997)

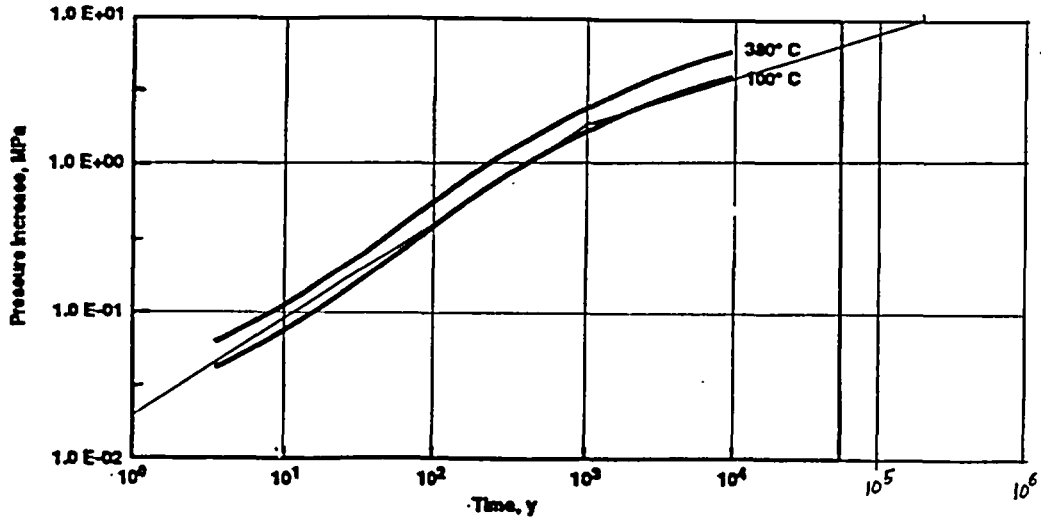


Figure 6. Helium Pressure from Alpha Decay (From Manaktala 1993)

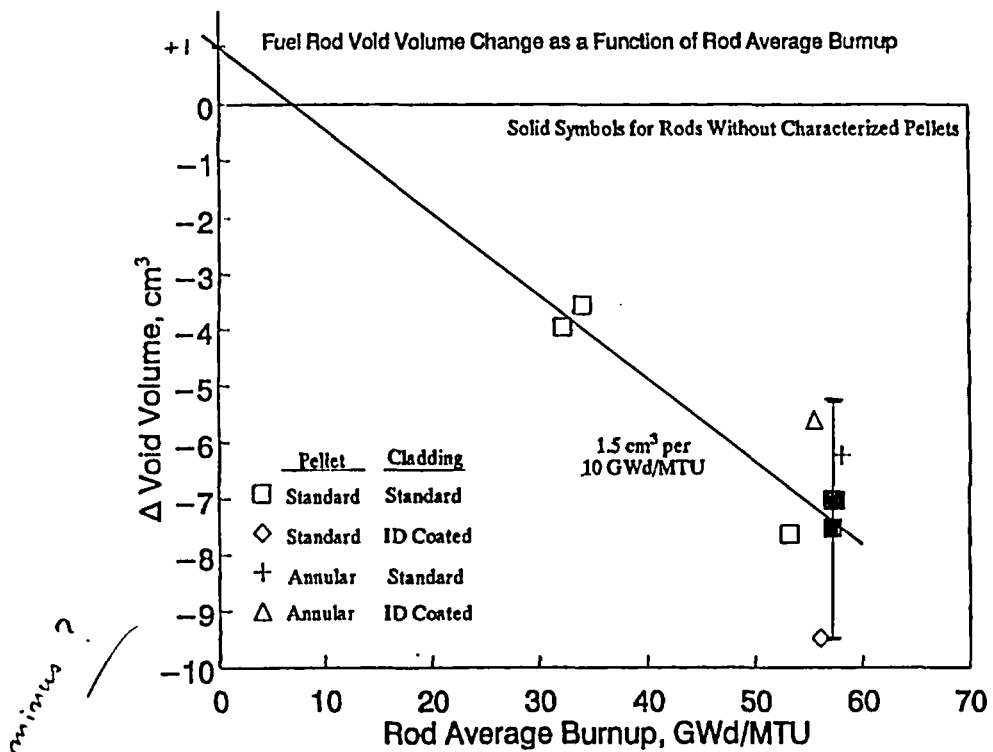


Figure 7. Fuel Rod Void Volume Change as a Function of Rod Average Burnup (from Smith et al. 1994)

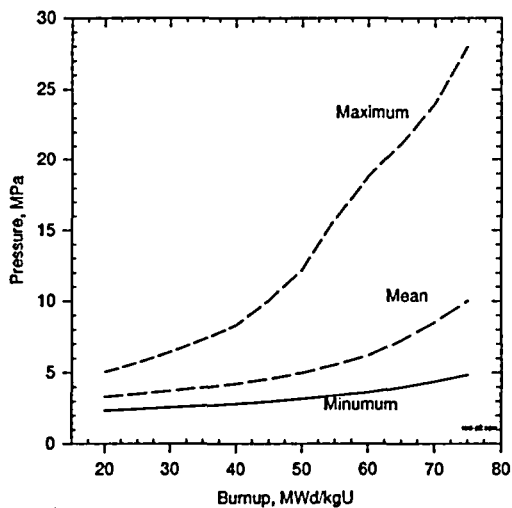


Figure 8. Rod Internal Pressure vs. Burnup

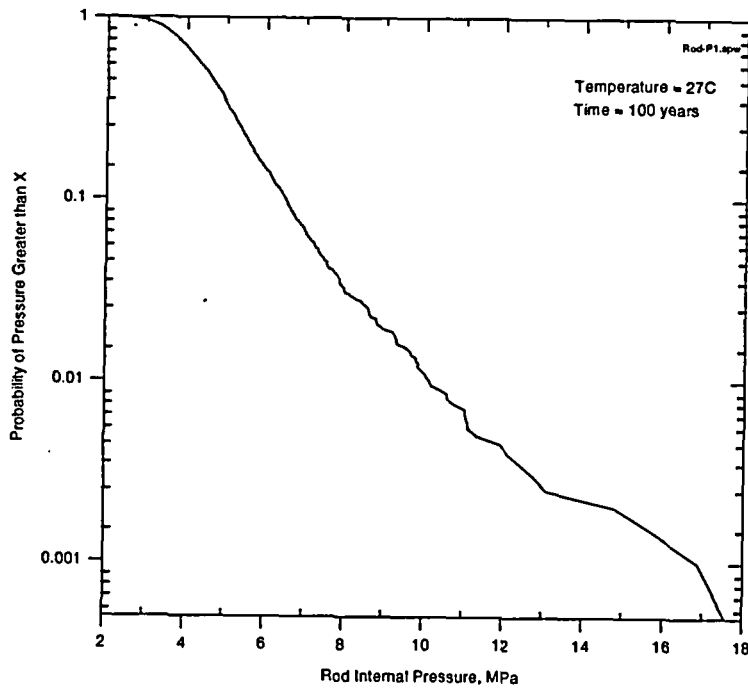


Figure 9. CCDF for Rod Internal Pressure

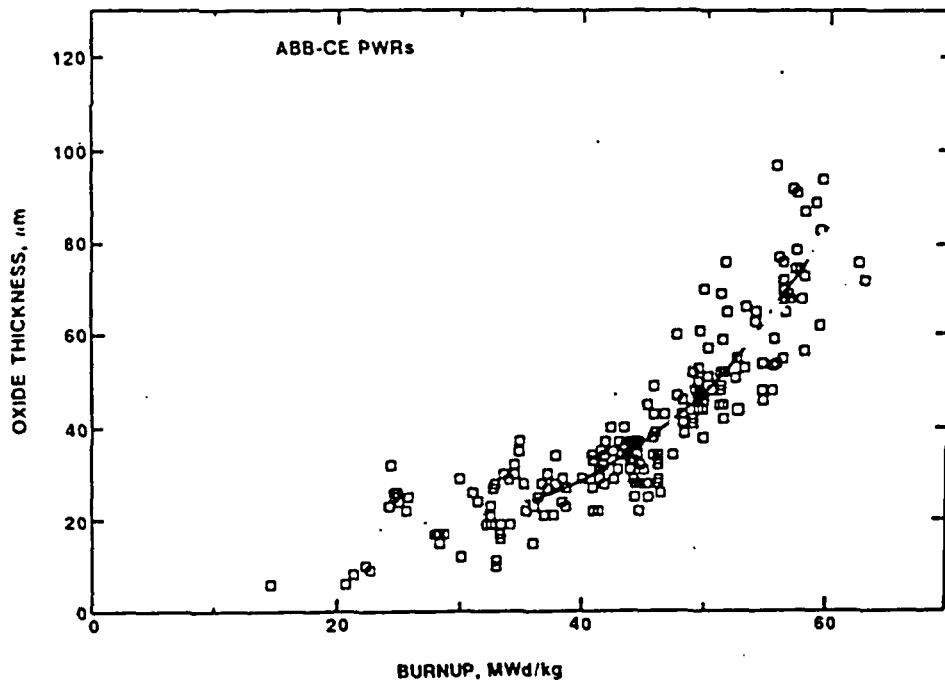


Figure 10. Cladding Oxide thickness vs. Burnup Reported by Garde (1991)

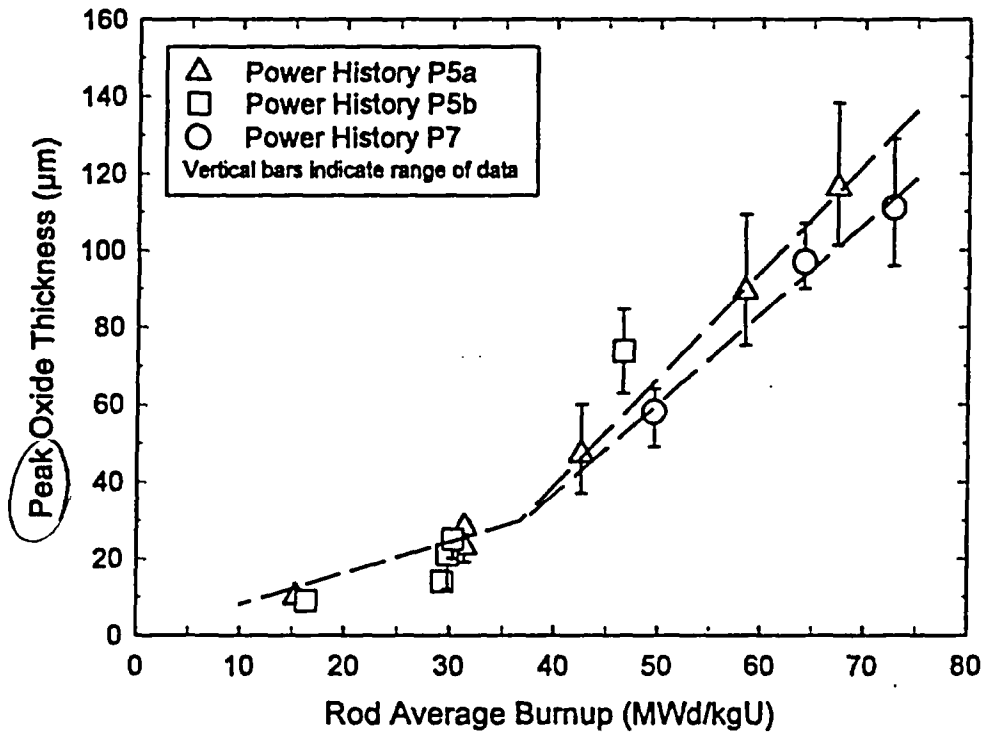


Figure 11. PWR Fuel Rod Oxide Thickness for High Burnup Fuels (from Van Swam et al. 1997a)

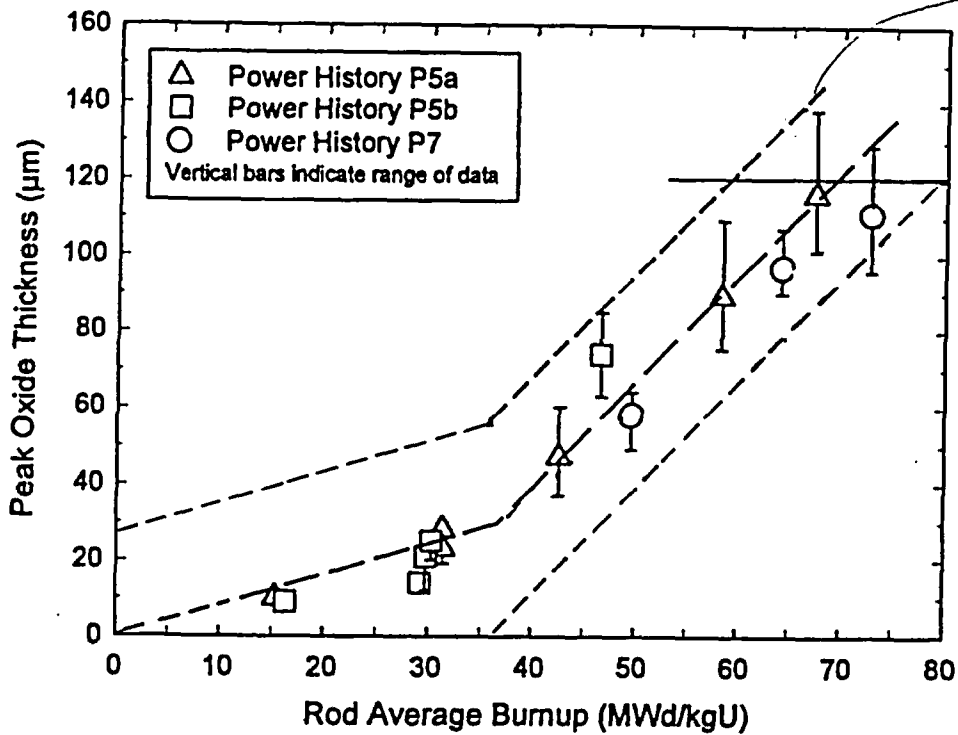


Figure 12. Mean Oxide Thickness and Range vs. Burnup

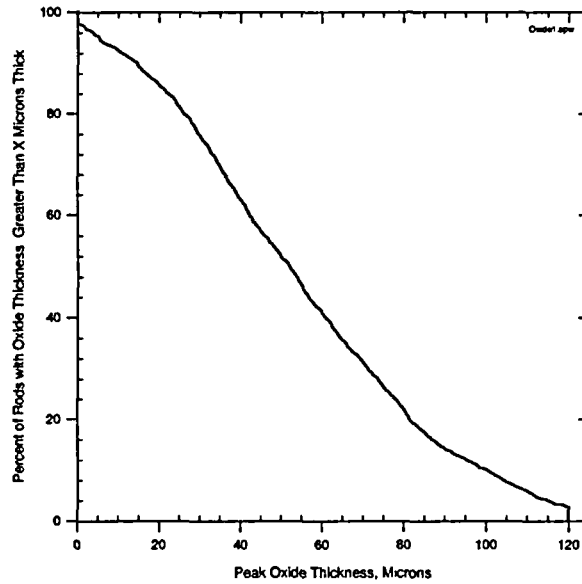


Figure 13. CCDF for Peak Rod Oxide Thickness

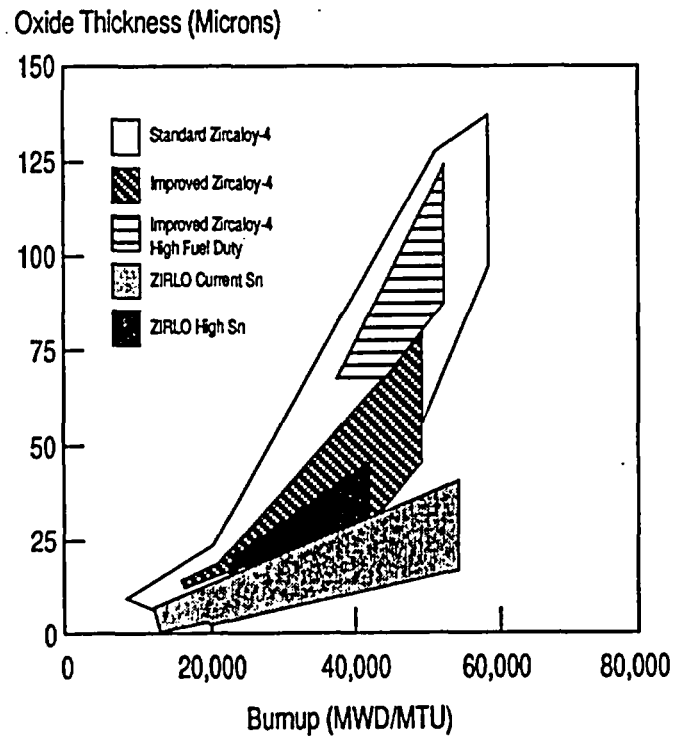


Figure 14. Corrosion: Oxide Thickness vs. Burnup for Alternative Fuel Rod Cladding Materials

(From Wilson et al. 1997)

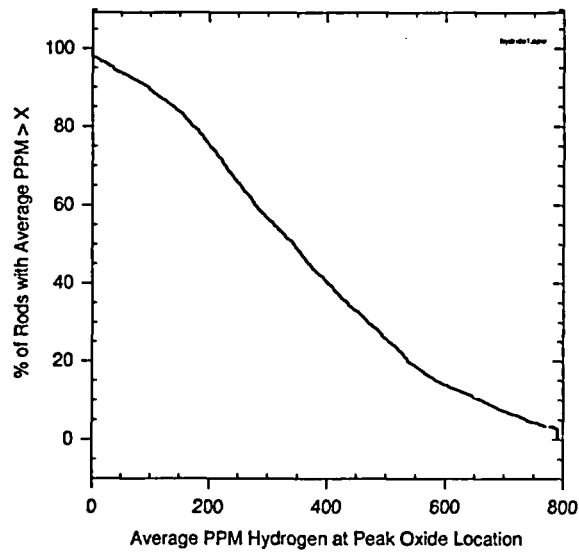


Figure 15. CCDF for Hydrogen Concentrations in PWR Fuel Rods

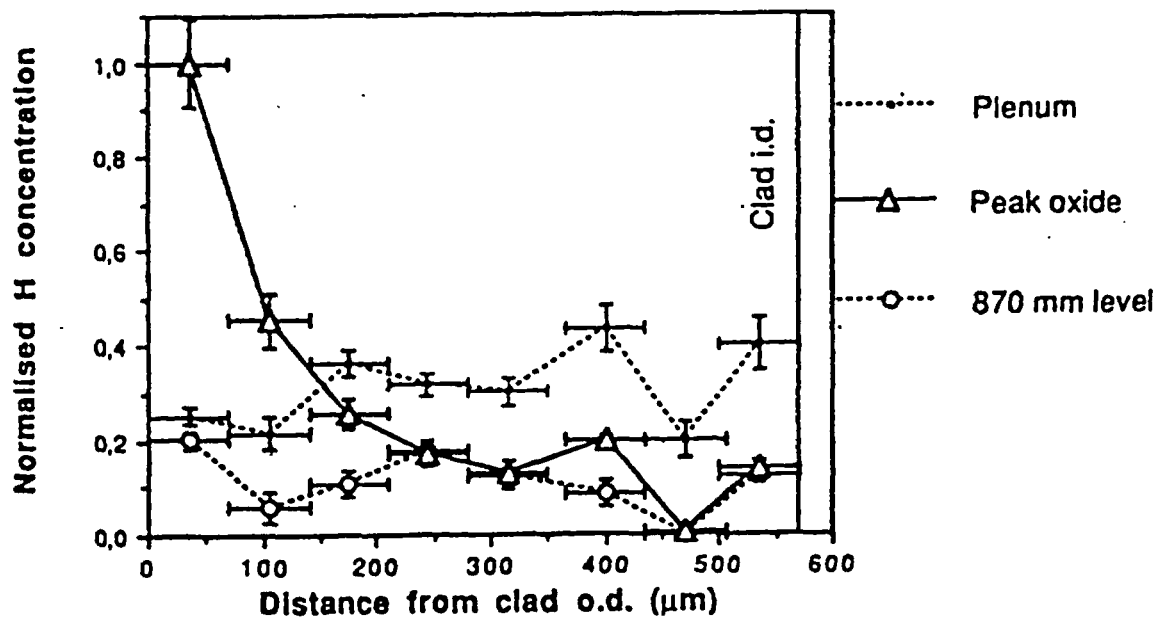


Figure 16. Cladding Radial Hydride Profiles (From Schrire et al. 1994)

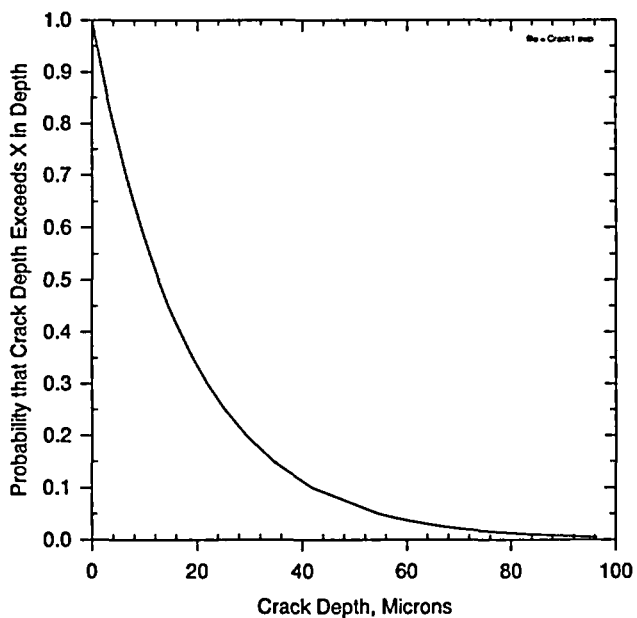


Figure 17. Crack Size Distribution for PWR Rods

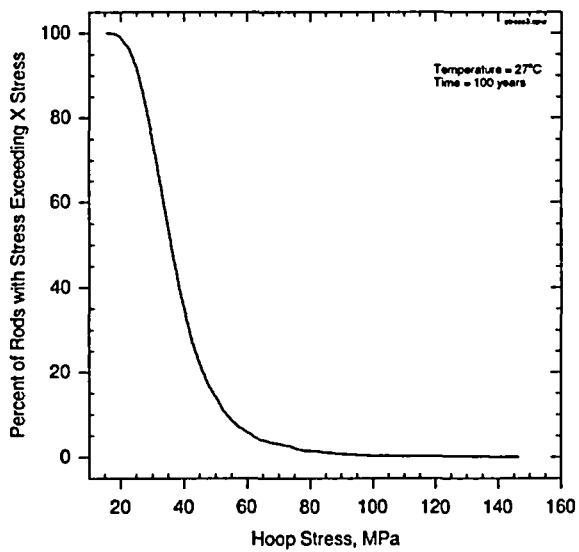


Figure 18. CCDF for Cladding Stress

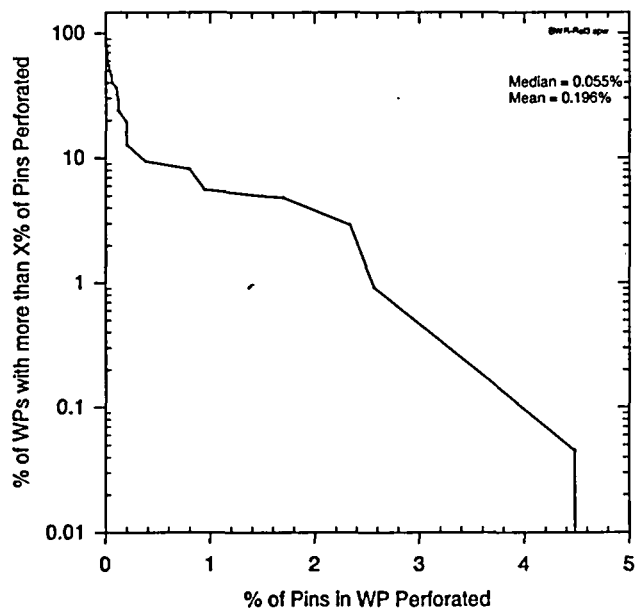


Figure 19. BWR: Distribution of Failed Rods in WPs

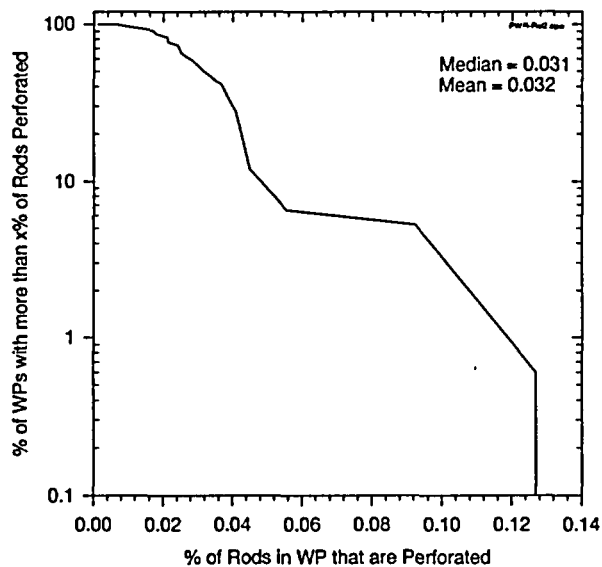


Figure 20. PWR: Distribution of Failed Rods in WPs

*page 65
66*

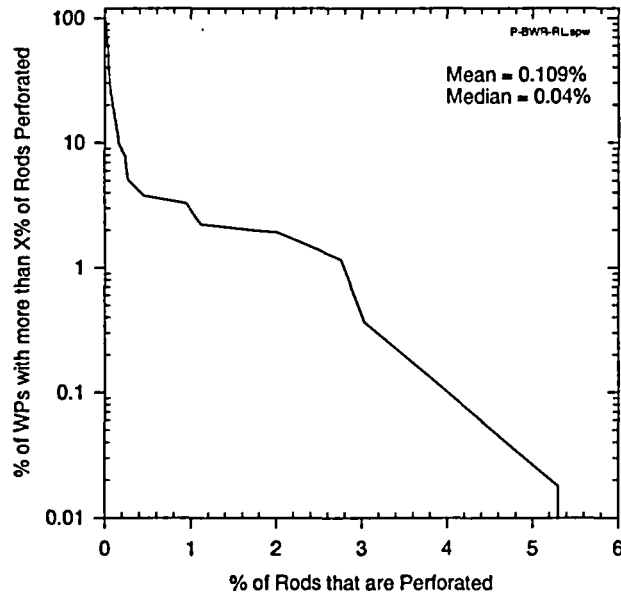


Figure 21. CCDF for Combined BWR & PWR Perforated Rods

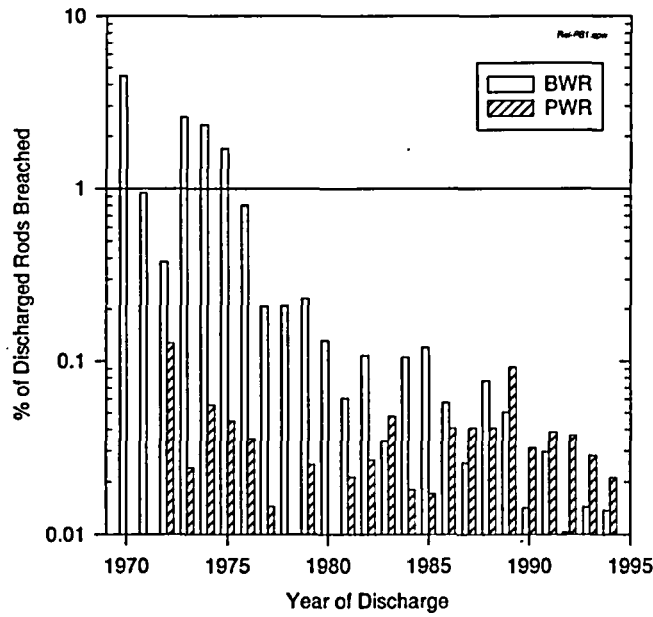


Figure 22. Fuel Reliability as a Function of Calendar Year

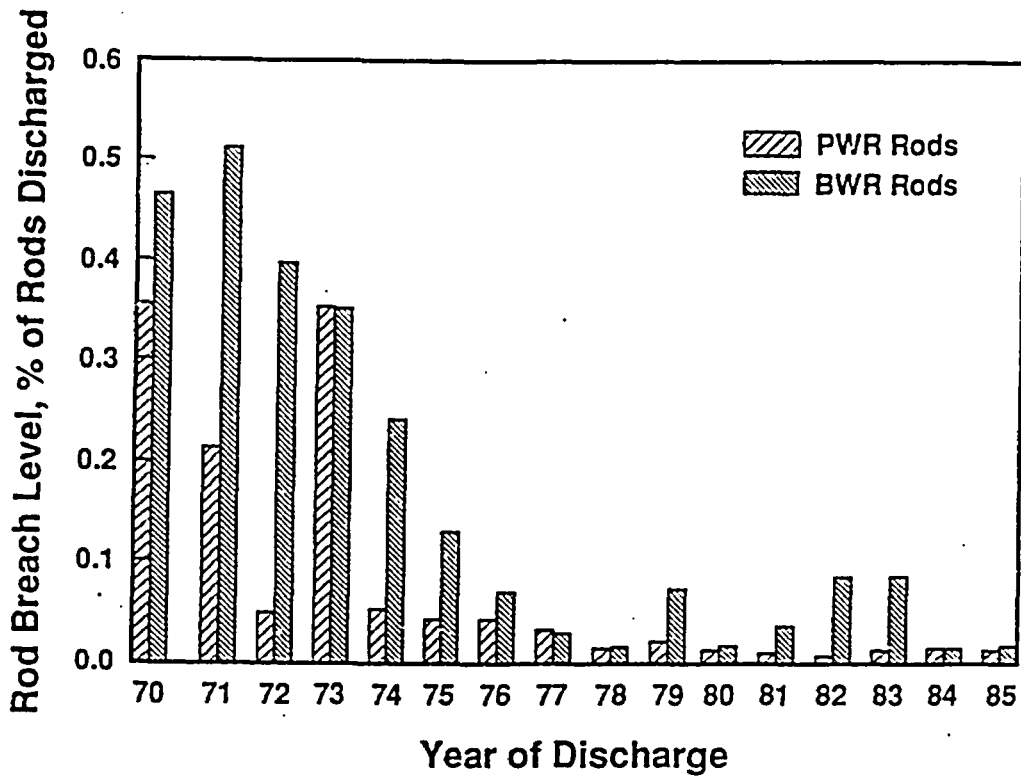


Figure 23. Fuel Rod Reliability Reported by Sanders et al. (1992)

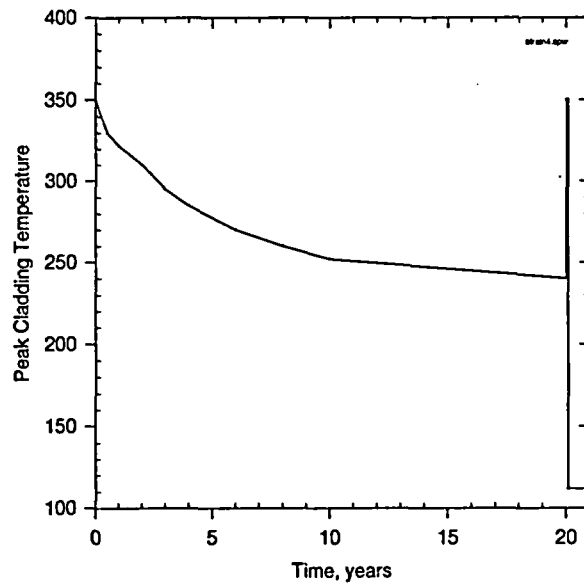


Figure 24. Temperature History Representing Dry Storage and Transportation

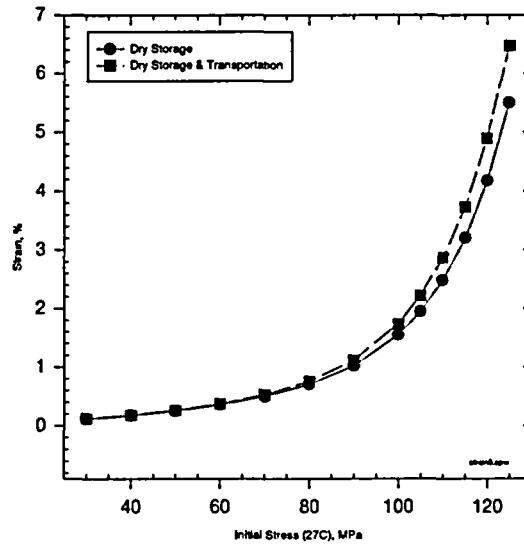


Figure 25. Cladding Creep Strain from Dry Storage and Transportation

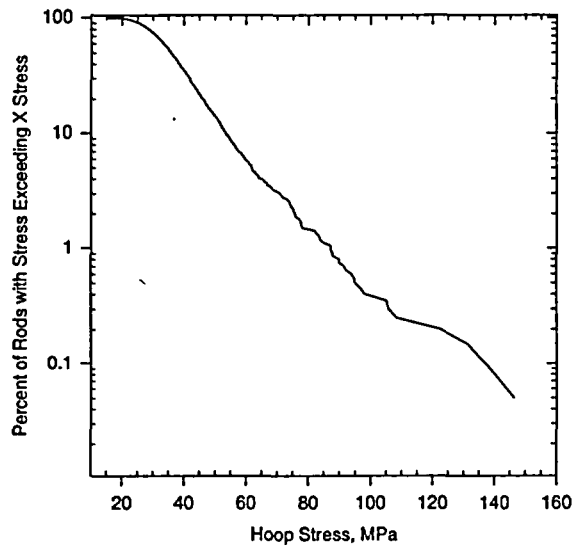


Figure 26. Details of CCDF for High rod Stress

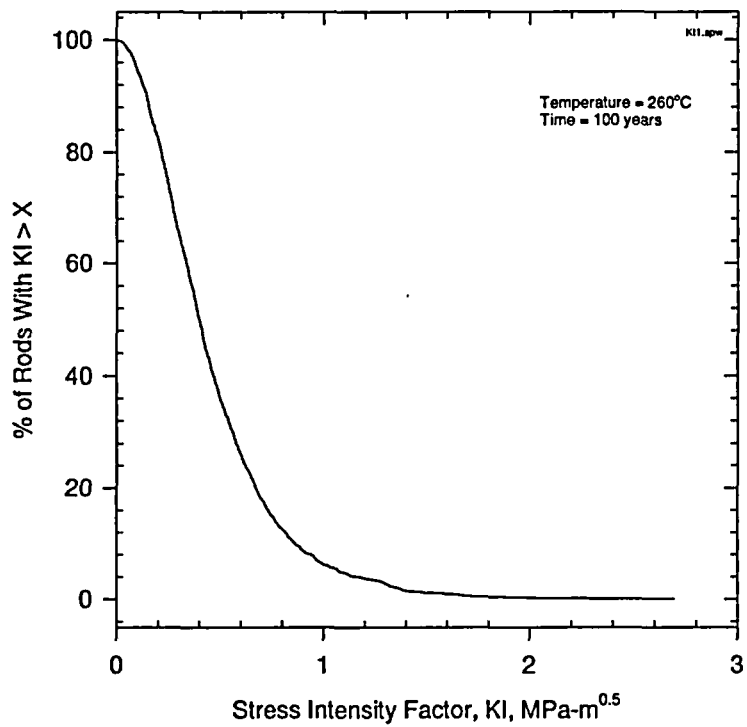


Figure 27. CCDF for Rod Stress Intensity Factors

9. ATTACHMENTS

The attachments are listed as follows:

| Attachment | Title | Pages |
|-------------------|---|--------------|
| I | List of Acronyms | 1 |
| II | Rod Failure during Reactor Operation | 4 |
| III | Description of Excel Spreadsheet: Rod-Initial-C.xls | 18 |